NMR and Computational Characterization of Mitomycin Cross-Linked to Adjacent Deoxyguanosines in the Minor Groove of the d(T-A-C-G-T-A)·d(T-A-C-G-T-A) Duplex†

David Norman,‡ David Live,§ Mallika Sastry,‡ Roselyn Lipman,∥ Brian E. Hingerty,⊥ Maria Tomasz,∥ Suse Broyde,# and Dinshaw J. Patel*,‡

Department of Biochemistry and Molecular Biophysics, College of Physicians and Surgeons, Columbia University, New York, New York 10032, Chemistry Department, Emory University, Atlanta, Georgia 30322, Department of Chemistry, Hunter College, City University of New York, New York, New York 10021, Health and Safety Research Division, Oak Ridge National Laboratory, Oak Ridge, Tennessee 37831, and Biology Department, New York University, New York, New York 10003

Received August 28, 1989; Revised Manuscript Received November 15, 1989

ABSTRACT: Two-dimensional homonuclear and heteronuclear NMR and minimized potential energy calculations have been combined to define the structure of the antitumor agent mitomycin C (MC) cross-linked to deoxyguanosines on adjacent base pairs in the d(T1-A2-C3-G4-T5-A6)·d(T7-A8-C9-G10-T11-A12) duplex. The majority of the mitomycin and nucleic acid protons in the MC-X 6-mer complex have been assigned from through-bond and through-space two-dimensional proton NMR studies in aqueous solution at 5 and 20 °C. The C3·G10 and G4·C9 base pairs are intact at the cross-link site and stack on each other in the complex. The amino protons of G4 and G10 resonate at 9.36 and 8.87 ppm and exhibit slow exchange with solvent H_2O. The NMR experimental data establish that the mitomycin is cross-linked to the DNA through the amino groups of G4 and G10 and is positioned in the minor groove. The conformation of the cross-link site is defined by a set of NOEs between the mitomycin H1″ and H2″ protons and the nucleic acid imino and amino protons of G4 and the H2 proton of A8 and another set of NOEs between the mitomycin geminal H10″ protons and the nucleic acid imino and amino protons of G10 and the H2 proton of A2. Several phosphorus resonances of the d(T-A-C-G-T-A) duplex shift dramaticaly on mitomycin cross-link formation and have been assigned from proton-detected phosphorus–proton two-dimensional correlation experiments. The proton chemical shifts and NOEs establish fraying at the ends of the d(T-A-C-G-T-A) duplex, and this feature is retained on mitomycin cross-link formation. The base–base and base–sugar NOEs exhibit similar patterns for symmetry-related steps on the two nucleic acid strands in the MC-X 6-mer complex, while the proton and phosphorus chemical shifts are dramatically perturbed at the G10-T11 step on cross-link formation. The NMR distance constraints have been included in minimized potential energy computations on the MC-X 6-mer complex. These computations were undertaken with the nonplanar five-membered ring of mitomycin in each of two pucker orientations. The resulting low-energy structures MX1 and MX2 have the mitomycin cross-linked in a widened minor groove with the chromophore ring system in the vicinity of the G10-T11 step on one of the two strands in the duplex. The experimental evidence supports this model since the H1′ of G10 is shifted dramatically upfield and the H1′ proton of T11 is shifted dramatically downfield on complex formation. The unconstrained final minimum energy conformations MX1 and MX2, which differ in the pucker of the five-membered ring of mitomycin, exhibit similar torsion angles at the bonds involved in covalent linkage of the antitumor agent to the DNA. However, there are large differences in several nucleic acid backbone torsion angles between conformations MX1 and MX2. A choice between them cannot be currently made since both MX1 and MX2 satisfy the available experiment NMR parameters for the MC-X 6-mer complex in solution.

Mitomycin (MC) (**1**) is an antitumor antibiotic agent which has been used clinically in treatment of a variety of cancers (Carter & Crooke, 1979). It also exhibits mutagenic activity (Balbinder & Kerry, 1984). The quinone, aziridine, carbinolamine, and carbamate functionalities are arranged in a unique compact structure in mitomycin (Hata et al., 1956; Wakaki et al., 1958; Webb et al., 1962). Mitomycin is an alkylating agent that binds covalently to DNA under both reductive (Szybalski & Iyer, 1967; Tomasz & Lipman, 1981) and acidic (Tomasz et al., 1985, 1987b) conditions.

The reductive alkylation adduct has been shown to result from a covalent linkage of the aziridine ring-opened mitomycin 1″ position with the N2 position of deoxyguanosine (Tomasz et al., 1986a,b, 1988). Models of this complex have been generated and energy minimized by using molecular mechanics computations without distance constraints (Rao et al., 1986; Verdine, 1986). By contrast, acidic activation results in covalent adduct formation at the N7 position of deoxyguanosine followed by either ring scission of the glycosidic bond or opening of the imidazole ring (Tomasz et al., 1987b).

Mitomycin is also known to cross-link DNA through bifunctional alkylation (Iyer & Szybalski, 1963) with cross-link formation favored over monoalkylation upon reductive acti-

† This research was supported by NIH CA-21111 (D.J.P.), NSF DMB-8604304 (D.L.), NIH CA-28681 and NIH RR-03037 Research Centers in Minority Institutions (M.T.), DOE Contract DE-AC05-840R21400 with Martin-Marietta Energy Systems (B.E.H.), and NIH CA-28038, DOE Contract DE-AC02-91ER60015, NSF DMB-8416009, and a Grand Challenge Award of supercomputer time DOE (S.B.).

‡ Columbia University.
§ Emory University.
∥ City University of New York.
⊥ Oak Ridge National Laboratory.
New York University.

0006-2960/90/0429-2861$02.50/0

vation with $Na_2S_2O_4$. Spectroscopic studies have established that the bisadduct involves covalent linkage through the mitomycin 1″ and 10″ positions to the two deoxyguanosine N2 positions on partner strands **2** in a (C-G)·(C-G) segment of

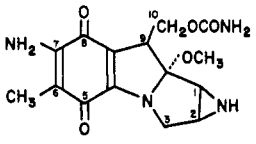

1

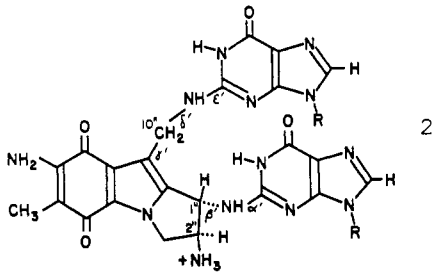

2

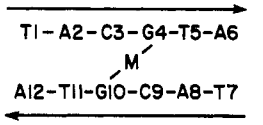

3

a DNA helix (Tomasz et al., 1987a; Chawla et al., 1987). The specificity for mitomycin cross-linking to (C-G)·(C-G) sites over (G-C)·(G-C) sites has been independently demonstrated through a gel electrophoresis binding assay (Teng et al., 1989). Further, the efficiency of cross-linking was shown to be dependent on local DNA structure (Cera & Crothers, 1989). Energy-minimized models generated without distance constraints of the mitomycin cross-link to a (C-G)·(C-G) step show no significant distortion of the DNA helix (Verdine, 1986; Tomasz et al., 1987a).

A definitive determination of the solution structure of mitomycin covalent adducts and cross-links can be approached by NMR characterization of the complex at the oligomer duplex level combined with energy minimization computational studies guided by the NMR interproton distance parameters as input constraints. This paper focuses on a combined NMR and computational study of mitomycin cross-linked to adjacent guanosines in the self-complementary d(T1-A2-C3-G4-T5-A6)·d(T7-A8-C9-G10-T11-A12) duplex (MC-X 6-mer complex) **3**.

Experimental Procedures

Oligonucleotide Synthesis. The oligonucleotide d(T-A-C-G-T-A) was synthesized on a Beckman System 1+ automated DNA synthesizer using a solid-phase cyanoethyl phosphoramidite approach. The crude 5′-dimethoxytritylated oligonucleotides were isolated by treatment of the support with concentrated aqueous ammonia for 36 h at room temperature. Purification of the products was by reverse-phase HPLC in two stages followed by desalting on Sephadex G-25. The oligomers were finally converted to sodium form by passage through a short column of Dowex 50X8 sodium form cation-exchange resin.

Synthesis and Purification of MC-X 6-mer Complex. The self-complementary hexanucleotide d(T-A-C-G-T-A) (100 A_{260} units; 1.6 μmol, based on ϵ_{260} = 63 000) and MC (**1**) (55 μmol) were mixed in 3.35 mL of 0.1 M Tris, pH 7.4, buffer. The solution was cooled in an ice bath and deaerated by bubbling helium gas. A deaerated solution of $Na_2S_2O_4$ in the above buffer (0.15 mL; 570 mM; 85 μmol) was then added in five equal increments at 10-min intervals and bubbling of helium continued through the reaction mixture for 60 min of total reaction time. This was followed by bubbling air for 5 min. The reaction mixture was chromatographed over a column of Sephadex G-25 (fine) (5 × 56 cm), 0.02 M NH_4HCO_3 eluant. The cross-linked adduct **3** (MC-X 6-mer complex) was eluted in the void volume (V_e = 480 mL), followed by the parent oligonucleotide (V_e = 580 mL). The crude **3** (approximately 30% yield on the basis of parent oligonucleotide) was purified to homogeneity by HPLC, using a C-3 reversed-phase column (1.0 × 25 cm; Beckman Ultrapore). A 5–11.2% linear gradient of acetonitrile in 0.1 M tetraethylammonium acetate, pH 7.0 (50 min, 5 mL/min flow rate), eluted **3** at 27 min. The yield after HPLC was approximately 15%, on the basis of the original hexanucleotide. The identity of **3** was established by ultraviolet spectra and analysis of its nuclease digest.

Characterization of MC-X 6-mer Complex. The fact that at room temperature **3** eluted at the void volume of the Sephadex G-25 column, i.e., earlier than the parent oligonucleotide, indicated qualitatively that **3** had increased molecular weight. The ultraviolet spectrum of **3** showed the characteristic mitosene absorption pattern in the 300–400-nm region (λ_{max} at 312 nm, shoulder at 350 nm; Tomasz et al., 1983). Enzymatic digestion by snake venom diesterase and alkaline phosphatase (3 units each per A_{260} unit oligonucleotide, in 0.02 M Tris–0.04 M $MgCl_2$, pH 8.2, 45 °C, 4 h) followed by HPLC analysis gave the following results: molar ratios dC/dG/dT/dA = 1:0:2:2 (±0.1). The peak at 48 min was shown to be **3** by mixed HPLC comparison with an authentic standard (Tomasz et al., 1987). These data indicate that the deoxyguanosines were modified while the other bases remained intact, and the modification corresponded to the cross-linked adduct **3**.

The circular dichroism spectra in the 200–300-nm region of the MC-X 6-mer complex **3** is complex and vastly altered compared to that of the parent hexanucleotide. The melting curve measured optically is broadened, and the T_m is increased in 1 M NaCl, compared to that of the parent hexanucleotide (28 and 22 °C, respectively). This is consistent with the greatly increased thermal stability of polynucleotides and DNA cross-linked by MC (Chawla et al., 1987). A more detailed report on the properties of the MC-X 6-mer complex **3** and similar complexes of longer oligonucleotides has been submitted for publication (Borowy-Borowski et al., 1990).

Proton NMR Studies. One- and two-dimensional proton NMR data sets were recorded on Bruker AM 400 and AM 500 spectrometers. Proton chemical shifts were referenced relative to internal 3-(trimethylsilyl)propionate-*2,2,3,3-d*$_4$ (TSP). Phase-sensitive two-dimensional proton NOESY spectra in D_2O were collected with a 2.0-s repetition time, a sweep width of 4000 Hz, and a mixing time of 300 ms. The carrier frequency was placed on the residual HOD resonance, which was irradiated with the decoupler channel. The data sets were collected with 512 t_1 experiments using 1024 complex data points in the t_2 dimension and 32 scans per t_1 increment. Real and imaginary data points were acquired sequentially and then merged to yield 256 complex t_1 points. The data sets were apodized with a 90° sine bell function, and 3-Hz line broadening was used in both dimensions. Magnitude two-dimensional proton-correlated (COSY) experiments were recorded with quadrature detection in both dimensions. The data sets were collected with 512 t_1 increments and a sweep width of 4000 Hz using 1024 complex data points in the t_2 dimension. A repetition delay of 1.0 s and 32 scans per t_1 increment were used. The data sets were apodized with an

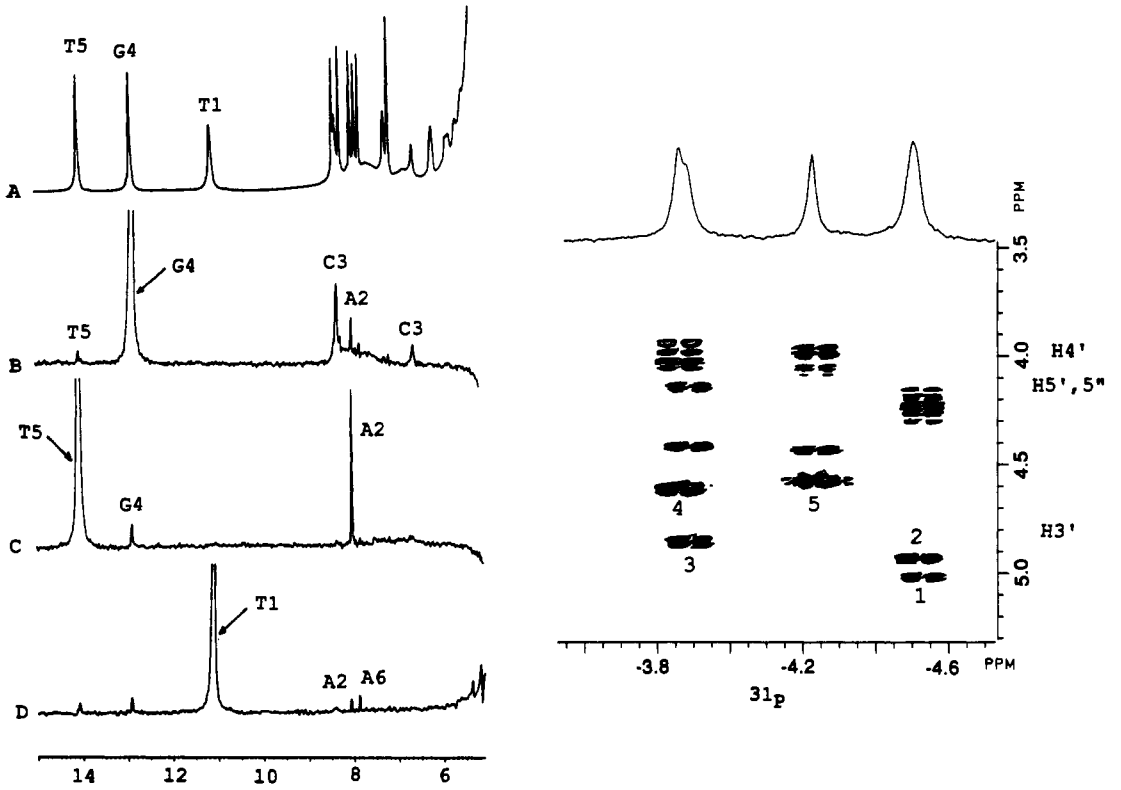

FIGURE 1: (Left panel) Proton NMR spectrum (7.0–15.0 ppm) of (A) the 6-mer duplex in H_2O buffer, pH 5.3, at 2 °C. One-dimensional NOE difference spectra are recorded following saturation of (B) the 12.89 ppm G4 imino proton, (C) the 14.06 ppm T5 imino proton, and (D) the 11.12 ppm T1 imino proton. (Right panel) Contour plot of the proton-detected phosphorus–proton heteronuclear COSY experiment on the 6-mer duplex in D_2O buffer, pH 5.3 at 5 °C. The phosphorus dimension extends from −3.7 to −4.7 ppm with the one-dimensional phosphorus spectrum recorded over the contour plot. The proton dimension extends from 3.8 to 5.2 ppm and encompasses the sugar H4′, H5′,5″ protons (3.8–4.5 ppm) and the sugar H3′ protons (4.5–5.1 ppm).

unshifted sine bell function zeroed to the 512th point and Fourier transformed in both dimensions.

Phosphorus NMR Studies. Phase-sensitive two-dimensional proton-detected phosphorus–proton COSY spectra were recorded with a 5-mm proton reverse detection probe and a broad-band decoupler accessory on a General Electric GN 500 spectrometer. The pulse sequence in the heteronuclear two-dimensional experiments was as described previously (Sklenar et al., 1986) except for the receiver phase cycling which should be corrected to sequence B in Sklenar and Bax (1987). A string of 34 (n = 34) 180° pulses separated by a d value of 50 ms was used in the beginning of the sequence to saturate the protons, and a postacquisition delay of 100 ms was used before the sequence was restarted. Alternate acquisitions were deposited in alternate memory blocks and were processed to give phase-sensitive two-dimensional spectra (States et al., 1982). For the two-dimensional data set, 256 scans were collected for each of 128 t_1 values used. Spectral width in the proton dimension was 2000 Hz in 1024 points, and the width in the phosphorus dimension was 1000 Hz in 128 points. The phosphorus dimension was zero filled twice in processing. The DM apodization function in the GN software was used with a value of 3 in both dimensions. Data were processed on the Nicolet 1280 computer on the spectrometer. Chemical shifts were referenced to trimethyl phosphate (TMP) in D_2O indirectly based on a measurement of a sample of TMP and TSP in D_2O and following the procedure for relating proton standard positions to that of another nucleus as described elsewhere (Live et al., 1984).

Computational Studies. Minimized potential energy calculations in torsion angle space were carried out with the program DUPLEX, which has been described in full detail previously (Hingerty et al., 1989). Full details of its application to the present problem are given in the supplementary material. These include implementation of novel approaches to generate coordinates for the mitomycin cross-link and incorporation of NOE-based distance constraints in the energy minimization algorithm.

Results

Mitomycin lacks an element of symmetry so that the twofold symmetry of the d(T1-A2-C3-G4-T5-A6) self-complementary duplex is lifted on mitomycin complex formation. Therefore, the sequence of one strand is labeled from T1 to A6 and the other strand from T7 to A12 in the MC-X 6-mer complex **3**.

We first outline the NMR parameters for the d(T-A-C-G-T-A) duplex since some uncharacteristic chemical shifts and NOE patterns are detected for this alternating pyrimidine–purine hexanucleotide duplex.

Exchangeable Protons in Duplex. The proton NMR spectrum (6–14 ppm) of the 6-mer duplex in H_2O buffer, pH 5.3 at 2 °C, is recorded in Figure 1A. The exchangeable imino resonances are detected at 14.06, 12.89, and 11.12 ppm and have been assigned from one-dimensional NOE experiments (left panel, Figure 1). We detect NOEs between the thymidine imino (14.06 ppm) and adenosine H2 (8.03 ppm) protons in the A2·T5 base pair (Figure 1C), between the guanosine imino (12.89 ppm) and the cytidine amino (8.36, 6.66 ppm) protons in the C3·G4 base pair (Figure 1B), and between the imino protons of adjacent A2·T5 and C3·G4 base pairs (Figure 1B,C). The remaining thymidine imino proton exhibits an unusual upfield chemical shift (11.12 ppm) and barely detectable NOE to the adenosine H2 protons (7.83 and 8.03 ppm) (Figure 1D). The imino and amino proton chemical shifts in the 6-mer duplex in H_2O buffer, pH 5.3 at 2 °C, are listed in Table I.

Table I: Exchangeable Proton, Nonexchangeable Proton, and Phosphorus Chemical Shifts in the 6-mer Duplex in 0.1 M NaCl and 10 mM Phosphate Solution

	exchangeable proton shifts (ppm), 2 °C			
base pair	G-N1H	T-N3H	C-N4H	A-H2
T1·A6		11.12		7.83
A2·T5		14.06		8.03
C3·G4	12.89		8.36, 6.66	

	nonexchangeable proton shifts (ppm), 10 °C						
base	H8	H6	H2	H5/CH_3	H1′	H2′,2″	H3′
T1		7.21		1.50	5.56	1.42, 1.95	4.52
A2	8.40		8.08		6.24	2.85, 2.90	4.96
C3		7.28		5.30	5.69	1.94, 2.39	4.79
G4	7.92				5.90	2.51, 2.57	4.86
T5		7.19		1.50	5.84	1.95, 2.10	4.54
A6	8.25		7.93		6.19	2.95, 2.64	4.65

step	cross peak	phosphorus shifts (ppm), 5 °C
T1-A2	5	−4.23
A2-C3	1	−4.53
C3-G4	3	−3.89
G4-T5	2	−4.52
T5-A6	4	−3.86

Nonexchangeable Protons in Duplex. The nonexchangeable protons in the d(T-A-C-G-T-A) duplex in D_2O buffer, pH 5.3 at 10 °C, have been assigned following analysis of NOESY (mixing time 300 ms) and COSY two-dimensional data sets. The expanded NOESY spectrum establishing distance connectivities between the base protons (7.2–8.6 ppm) and the cytidine H5 and sugar H1′ protons (5.2–6.4 ppm) is plotted in Figure 2A, while the expanded magnitude COSY spectrum establishing coupling connectivities between sugar H1′ and H3′ protons (4.1–6.4 ppm) and sugar H2′,2″ protons (1.4–3.2 ppm) is plotted in Figure 2B. The nonexchangeable proton resonances can be assigned from these data, and the base and sugar H1′, H2′,2″, and H3′ shifts are listed for the 6-mer duplex in D_2O buffer, pH 5.3 at 10 °C, in Table I. It should be noted that the NOEs between base protons and their 5′-flanking sugar H1′ protons are either weak or absent in the T1-A2 and T5-A6 steps in the 6-mer duplex (Figure 2A).

Phosphorus Resonances in Duplex. The phosphorus resonances in the d(T-A-C-G-T-A) duplex in D_2O buffer, pH 5.3, 5 °C, are dispersed between −3.85 and −4.53 ppm relative to standard trimethyl phosphate. The phosphorus resonances have been assigned through correlation with the known H3′ proton assignments in proton-detected phosphorus–proton heteronuclear correlation experiments as shown in the contour plot in Figure 1 (right panel). The phosphorus chemical shifts are listed in Table I with internucleotide phosphates at pyrimidine–purine C3-G4 and T5-A6 steps resonating at low field and those at purine–pyrimidine A2-C3 and G4-T5 steps resonating at high field in the 6-mer duplex.

Exchangeable Protons in Complex. The proton spectra (7.0–14.0 ppm) of the MC-X 6-mer complex in H_2O buffer, pH 5.0, at −1, 10, and 24 °C, are recorded in Figure 3A. Resolved exchangeable protons are detected between 12.6 and 13.5 ppm, between 10.8 and 11.5 ppm, and between 8.8 and 9.4 ppm (Figure 3A).

The imino and substituted amino protons of deoxyguanosine can be readily identified from the strong NOEs detected between these protons in one-dimensional NOE difference spectra recorded at pH 5.0 and −1 °C (Figure 4B–I). There is a single deoxyguanosine on each strand, and we arbitrarily assign the 13.12 ppm deoxyguanosine imino proton to G4 and the 12.60 ppm deoxyguanosine imino proton to G10 in the MC-X 6-mer complex.

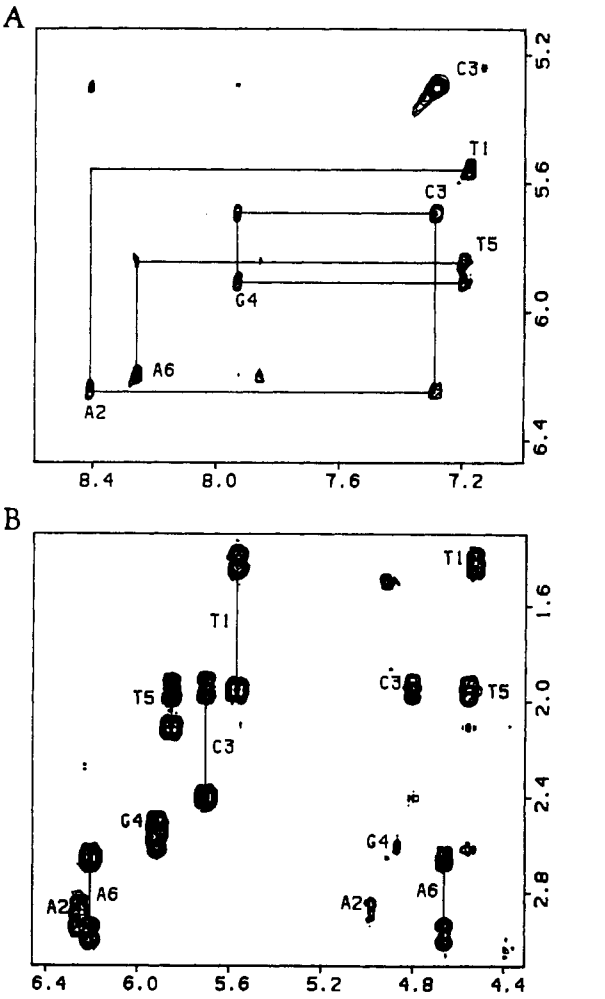

FIGURE 2: Expanded contour plots establishing (A) distance connectivities between the base protons (7.2–8.6 ppm) and the sugar H1′ and cytidine H5 protons (5.2–6.4 ppm) in the phase-sensitive NOESY (300-ms mixing time) spectrum and (B) coupling connectivities between sugar H1′ and H3′ protons (4.1–6.4 ppm) and sugar H2′,2″ protons (1.4–3.2 ppm) in the magnitude COSY spectrum of the 6-mer duplex in D_2O buffer, pH 5.3, at 10 °C. The tracing in (A) follows connectivities between adjacent base protons through their intervening sugar H1′ protons.

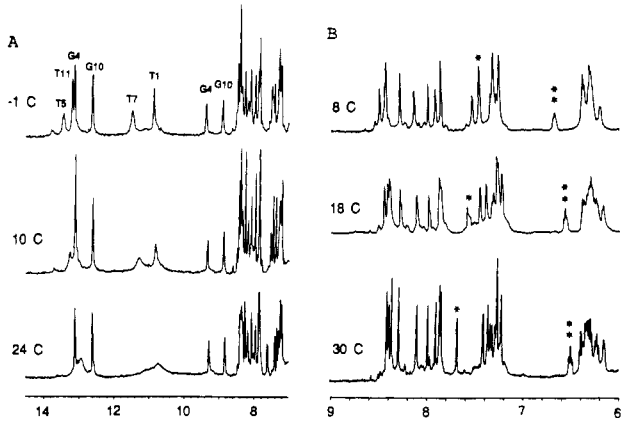

FIGURE 3: (A) Proton NMR spectra (7.0–14.5 ppm) of the MC-X 6-mer complex in H_2O buffer, pH 5.0, at −1, 10, and 23 °C. (B) Proton NMR spectra (6.0–9.0 ppm) of the MC-X 6-mer complex in D_2O buffer, pH 6.9, at 8, 18, and 30 °C. The H2 proton of A6 is designated by an asterisk, while the H1′ proton of T11 is designated by a double asterisk.

Saturation of the 13.12 ppm deoxyguanosine imino proton of G4 exhibits NOEs to the hydrogeh-bonded amino protons of G4 (9.36 ppm) and C9 (8.15 ppm) within the G4·C9 base

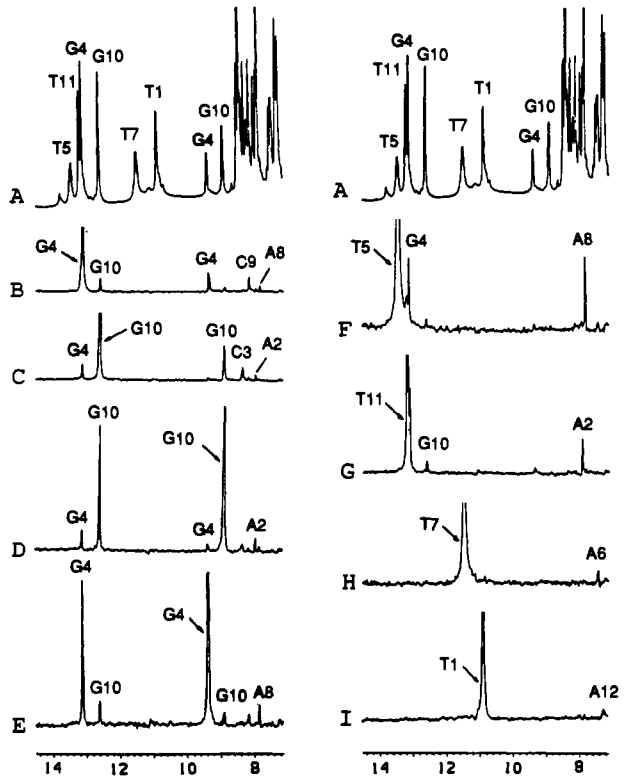

FIGURE 4: (A) Proton NMR spectrum (7.0–14.0 ppm) of the MC-X 6-mer complex in H_2O buffer, pH 5.0, at −1 °C. One-dimensional NOE difference spectra are recorded following saturation of (B) the 13.12 ppm G4 imino proton, (C) the 12.60 ppm G10 imino proton, (D) the 8.87 ppm G10 amino proton, (E) the 9.36 ppm G4 amino proton, (F) the 13.45 ppm T5 imino proton, (G) the 13.19 ppm T11 imino proton, (H) the 11.48 ppm T7 imino proton, and (I) the 10.86 ppm T1 imino proton.

pair and NOEs to the imino protons of G10 and the H2 proton of A8 of adjacent C3·G10 and T5·A8 base pairs (Figure 4B). Similarly, saturation of the 12.60 ppm deoxyguanosine imino proton of G10 exhibits NOEs to the hydrogen-bonded amino protons of G10 (8.87 ppm) and C3 (8.33 ppm) within the C3·G10 base pair and NOEs to the imino protons of G4 and the H2 proton of A2 of adjacent G4·C9 and A2·T11 base pairs (Figure 4C). NOEs are also detected between the amino proton of G10 and the imino proton of G4 (Figure 4D) and between the amino proton of G4 and the imino proton of G10 (Figure 4E) in the MC-X 6-mer complex. By contrast, weaker NOEs are detected between the amino protons of G4 and G10 (Figure 4D,E) in the MC-X 6-mer complex.

Two thymidine imino protons are detected to low field at 13.45–13.19 ppm with the former exhibiting a greater line width than the latter in the MC-X 6-mer complex, pH 5.0 at −1 °C (Figure 4A). The 13.45 ppm imino proton is assigned to T5 since it exhibits an NOE to the H2 of A8 within the T5·A8 base pair (Figure 4F), while the 13.19 ppm imino proton is assigned to T11 since it exhibits an NOE to the H2 proton of A2 within the A2·T11 base pair (Figure 4G). An NOE is detected between the imino protons of adjacent T5·A8 and G4·C9 base pairs (Figure 4F), and a weaker NOE is detected between the imino protons of adjacent A2·T11 and C3·G10 base pairs (Figure 4G) in the MC-X 6-mer complex.

The remaining thymidine imino protons resonate upfield at 11.48 and 10.86 ppm with the former exhibiting a greater line width than the latter in the MC-X 6-mer complex, pH 5.0 at −1 °C (Figure 4A). The deoxyadenosine H2 protons of A6 and A12 can be independently assigned on the basis of NOEs to sugar H1′ protons (see below). The 11.48 ppm imino proton is assigned to T7 since it exhibits a very weak NOE to the H2 proton of A6 within the A6·T7 base pair (Figure 4H), while the 10.86 ppm imino proton is assigned to T1 since it exhibits a very weak NOE to the H2 proton of A12 within the T1·A12 base pair (Figure 4I) in the MC-X 6-mer complex.

Table II: Exchangeable Proton Chemical Shifts in the MC-X 6-mer Complex in 0.1 M NaCl, 10 mM Phosphate, and H_2O, pH 5.0, −1 °C

	chemical shifts (ppm)				
base pair	G-N1H	T-N3H	G-N2H[a]	C-N4H[a]	A-H2
T1·A12		10.86			7.31
A2·T11		13.19			7.95
C3·G10	12.60		8.87	8.33	
G4·C9	13.12		9.36	8.15	
T5·A8		13.45			7.83
A6·T7		11.48			7.46

Phosphorus Chemical Shifts in the MC-X 6-mer Complex in 0.1 M NaCl, 10 mM Phosphate, and D_2O

	complex		
assignment	cross peak	5 °C	20 °C
T1-A2	10	−4.35	−4.33
A2-C3	2	−4.62	−4.57
C3-G4	6	−3.44	−3.58
G4-T5	1	−4.17	−4.06
T5-A6	5	−3.69	−3.88
T7-A8	9	−4.45	−4.41
A8-C9	3	−4.45	−4.45
C9-G10	8	−3.72	−3.76
G10-T11	4	−3.68	−3.76
T11-A12	7	−3.66	−3.69

[a] Hydrogen-bonded pair.

The imino and amino exchangeable proton chemical shifts in the MC-X 6-mer complex in H_2O buffer, pH 5.0 at −1 °C, are listed in Table II.

The temperature dependence of the imino and amino proton chemical shifts (8–14 ppm) of the MC-X 6-mer complex in H_2O buffer, pH 5.0 between −1 and 24 °C (Figure 3A), establishes that all the thymidine imino protons shift upfield and broaden with increasing temperature. By contrast, the chemical shifts and line widths of the deoxyguanosine imino and amino protons at the mitomycin cross-link site remain unperturbed when the temperature is raised from −1 to 24 °C.

Nonexchangeable Protons in Complex. The nonexchangeable proton spectra (1.0–9.0 ppm) of the MC-X 6-mer complex in D_2O buffer, pH 6.9, at 8, 18, and 30 °C, are plotted in Figure 3B. The proton resonances are narrow and well resolved and amenable to analysis by two-dimensional NMR methods.

The slowly exchanging amino protons of deoxyguanosine at the cross-link site resonate at 9.35 and 8.88 ppm and are detected in freshly dissolved samples of the MC-X 6-mer complex in D_2O solution. These guanosine amino protons exhibit through-space and through-bond connectivities to mitomycin protons as observed in expanded phase-sensitive NOESY (Figure 5A) and magnitude COSY (Figure 5B) spectra of the MC-X 6-mer complex. Specifically, the 9.33 ppm amino proton of G4 exhibits connectivities to the 6.17 ppm H1″ proton of cross-linked mitomycin (peak B, Figure 5A,B) which in turn exhibits connectivities to the 4.28 ppm adjacent H2″ proton (peak E, Figure 5A,B). The 8.88 ppm amino proton of G10 exhibits connectivities to the 3.91 ppm (peak C, Figure 5A,B) and 5.05 ppm (peak D, Figure 5A,B) geminal H10″ protons of the cross-linked mitomycin which in turn are connected to each other (peak F, Figure 5A,B). These results establish the groups involved in cross-link formation between mitomycin and the nucleic acid in the MC-X 6-mer complex.

It is important to differentiate protons on the T1-A2-C3-

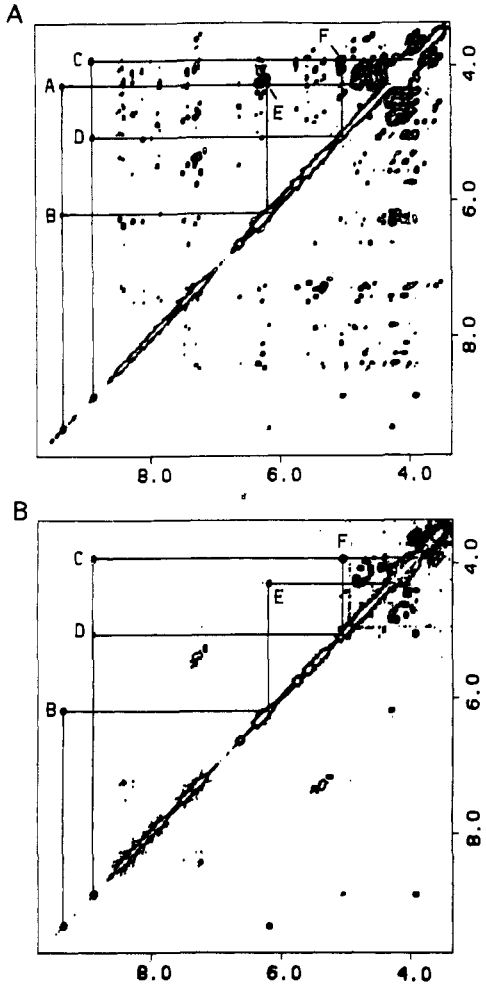

FIGURE 5: Expanded contour plots (symmetrical 3.5–10.0 ppm) establishing (A) distance connectivities in the phase-sensitive NOESY (300-ms mixing time) spectrum and (B) coupling connectivities in the magnitude COSY spectrum of the MC-X 6-mer complex in D_2O buffer, pH 6.9, at 5 °C. Cross peaks A–F are assigned as follows: A, G4(N2H)–MX(H2″); B, G4(N2H)–MX(H1″); C, G10-(N2H)–MX(H10″A); D, G10(N2H)–MX(H10″B); E, MX-(H1″)–MX(H2″); F, MX(H10″A)–MX(H10″B).

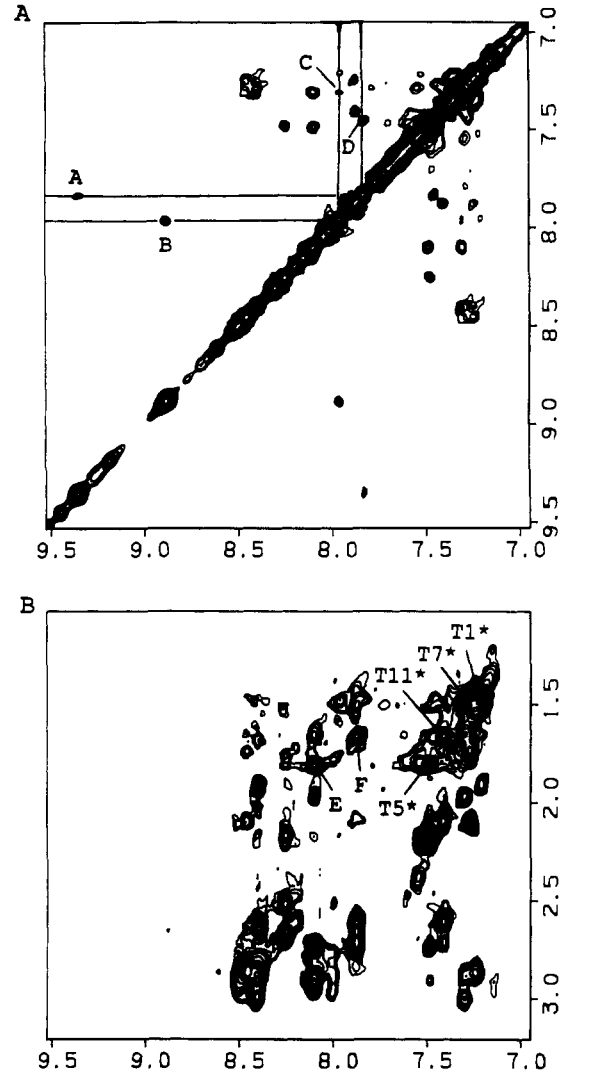

FIGURE 6: Expanded NOESY contour plots (300-ms mixing time) of the MC-X 6-mer complex in D_2O buffer, pH 6.9, 5 °C, establishing distance connectivities (A) in the symmetrical 6.0–9.6 ppm base proton region and (B) between the base proton region (6.0–9.6 ppm) and the sugar H2′,2″ and CH_3 proton region (1.2–3.2 ppm). The thymidine H6–CH_3 connectivities are designated by asterisks. Cross peaks A–F are assigned as follows: A, G4(N2H)–A8(H2); B, G10(N2H)–A2(H2); C, A2(H2)–A12(H2); D, A8(H2)–A6(H2); E, G4(H8)–T5(CH_3); F, G10(H8)–T11(CH_3). The thymidine H6–CH_3 NOEs are designated by asterisks.

G4-T5-A6 strand from their counterparts related by symmetry on the T7-A8-C9-G10-T11-A12 strand in the MC-X 6-mer complex. This has been approached by first differentiating between the H2 protons of A2·T11 and T5·A8 base pairs related by sequence symmetry on either side of the cross-link site. The deoxyadenosine H2 protons of A2, A6, A8, and A12 can be readily identified on the basis of the long spin relaxation times in the spectrum of the MC-X 6-mer complex. We detect an NOE between the amino proton of G4 and an H2 proton (peak A, Figure 6A) which must be assigned to adjacent A8 and another NOE between the amino proton of G10 and an H2 proton (peak B, Figure 6A) which must be assigned to adjacent A2 in the MC-X 6-mer complex. In addition, NOEs are detected between H2 protons on adjacent A·T base pairs with the NOE between the H2 protons of A6 and A8 (peak D, Figure 6A) stronger than that between the H2 protons of A2 and A12 (peak C, Figure 6A). This observation establishes structural differences between the (T1-A2)·(T11-A12) end and the (T5-A6)·(T7-A8) end of the MC-X 6-mer complex.

The deoxyadenosine H2 protons exhibit weak NOEs to adjacent sugar H1′ protons in right-handed B-form DNA. Thus, the H2 proton of A2 may exhibit NOEs to the H1′ protons of A2, C3, and A12 while the H2 proton of A8 may exhibit NOEs to the H1′ protons of A8, C9, and A6 in the MC-X 6-mer complex. Experimentally, the H2 proton of A2 exhibits a weak NOE to the H1′ proton of C3 (peak C, Figure 7A) which differentiates between positions C3 and C9 on the two strands. Similarly, the H2 proton of A8 exhibits a weak NOE to the H1′ proton of A6 (peak D, Figure 7A) which differentiates between positions A6 and A12 on the two strands.

The base proton (purine H8 and pyrimidine H6) to sugar H1′ NOE connectivities are traced for the T1–A6 strand in Figure 7A and are traced for the T7–A12 strand in Figure 7B in expanded contour plots of the NOESY (300-ms mixing time) spectra of the MC-X 6-mer complex at 5 °C. It is readily apparent that several NOE cross peaks between the base protons and their 5′-linked sugar H1′ protons are either weak or missing, with the effect most pronounced at the C3-G4 (Figure 7A) and C9-G10 (Figure 7B) steps near the cross-link site. There are also perturbations in the base to sugar H1′ connectivities in the T1-A2 and T5-A6 steps (Figure 7A) and in the T7-A8 and T11-A12 steps (Figure 7B).

NOEs are detected between adjacent purine H8 and py-

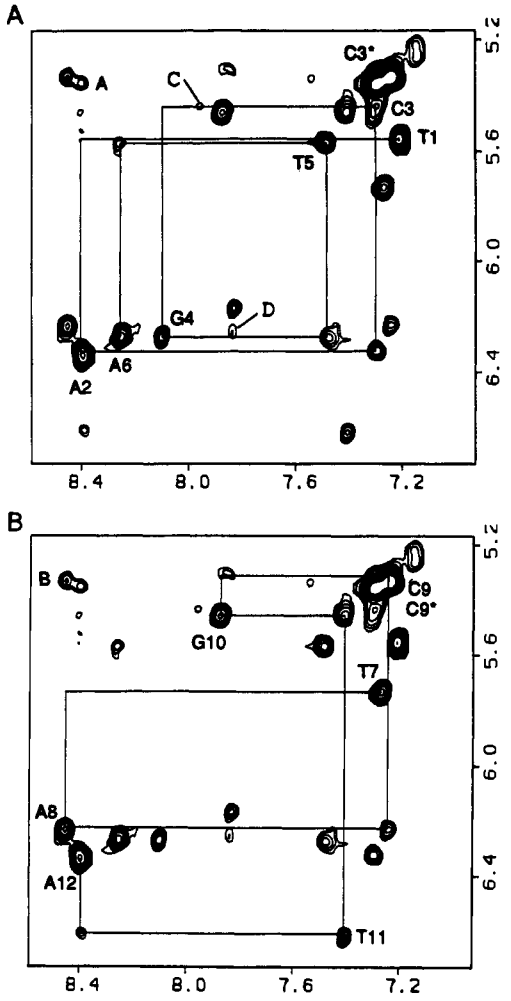

FIGURE 7: Expanded NOESY contour plots (300-ms mixing time) of the MC-X 6-mer complex D_2O buffer, pH 6.9, 5 °C, establishing distance connectivities between the base protons (7.0–8.5 ppm) and the sugar H1′ and cytidine H5 protons (5.2–6.7 ppm). The chain tracing in (A) is from T1 to A6 and in (B) is from T7 to A12. The tracing follows connectivities between adjacent base protons through their intervening sugar H1′ protons. The cytidine H5–H6 connectivities are designated by asterisks. Cross peaks A–D are assigned as follows: A, A2(H8)–C3(H5); B, A8(H8)–C9(H5); C, A3-(H2)–C3(H1′); D, A8(H2)–A6(H1′).

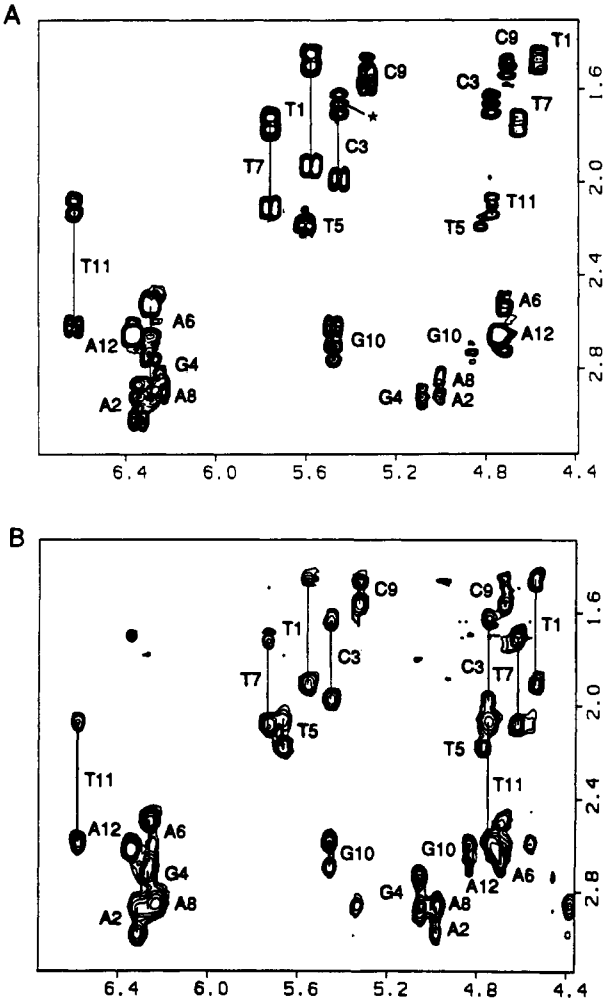

FIGURE 8: Expanded contour plots between the sugar H1′ and H3′ protons (4.4–6.8 ppm) and the sugar H2′,2″ protons (1.3–3.1 ppm) establishing (A) coupling connectivities in the magnitude COSY spectrum and (B) distance connectivities in the phase-sensitive NOESY (300-ms mixing time) spectrum of the MC-X 6-mer complex in D_2O buffer, pH 6.9, at 5 °C. The connectivities between sugar protons are assigned in the figure.

rimidine H5/CH_3 base protons in the purine(3′–5′)pyrimidine A2-C3 (peak A, Figure 7A), G4-T5 (peak E, Figure 6B), A8-C9 (peak B, Figure 7A), and G10-T11 (peak F, Figure 6B) steps in the MC-X 6-mer complex at 5 °C.

It should be noted that the sugar H1′ of G10 (5.46 ppm) is upfield from the chemical shifts (6.24–6.35 ppm) of the remaining purine (A2, G4, A6, A8, and A12) sugar H1′ protons, while the sugar H1′ of T11 (6.62 ppm) is downfield from the chemical shifts (5.31–5.74 ppm) of the remaining pyrimidine (T1, C3, T5, T7, and C9) sugar H1′ protons in the MC-X 6-mer complex at 5 °C (Figure 7).

The through-bond (Figure 8A) and through-space (Figure 8B) connectivities between the sugar H1′ (5.2–6.8 ppm) and the sugar H3′ (4.4–5.2 ppm) protons with the sugar H2′,2″ (1.4–3.2 ppm) protons are exceptionally well resolved and are helpful in unambiguously assigning the sugar H1′, H2′,2″, and H3′ protons in the MC-X 6-mer complex. There are some unusual H1′–H2′,2″ coupling patterns (asterisked cross peak corresponding to H1′–H2′ connectivity for C3, Figure 8A), and pattern reversals (labeled G10, Figure 8A) are detected in the magnitude COSY spectrum of the MC-X 6-mer complex.

A set of unexpected NOEs were detected between sugar protons on adjacent residues in the NOESY contour plot of the MC-X 6-mer complex in D_2O buffer at 5 °C. Specifically, a cross peak was observed between the sugar H1′ protons of G10 and T11 (peak A, Figure 9A), and another weaker NOE was observed between the H1′ protons of G4 and T5 (peak B, Figure 9A). These NOEs provide important constraints on the sugar rings at the cross-link site.

A set of NOEs have been identified between the mitomycin protons and the deoxyadenosine H2 protons in the expanded NOESY (300-ms mixing time) contour plot of the MC-X 6-mer complex in D_2O buffer at 5 °C. These intermolecular constraints include NOEs observed between the H2 proton of A8 and the mitomycin H1″ (peak D, Figure 9B) and H2″ (peak C, Figure 9B) protons and between the H2 proton of A2 and the geminal mitomycin H10″ protons (peaks A and B, Figure 9B).

The nonexchangeable base and sugar H1′, H2′,2″, and H3′ proton chemical shifts in the MC-X 6-mer complex in D_2O buffer, pH 6.9 at 5 °C, are listed in Table III. A parallel two-dimensional NMR study was undertaken on the MC-X 6-mer complex in D_2O at 20 °C. The contours in the 300-ms mixing time NOESY spectra are weak, while excellent COSY spectra were obtained on the narrow resonances at this elevated temperature. The nonexchangeable proton chemical shifts on

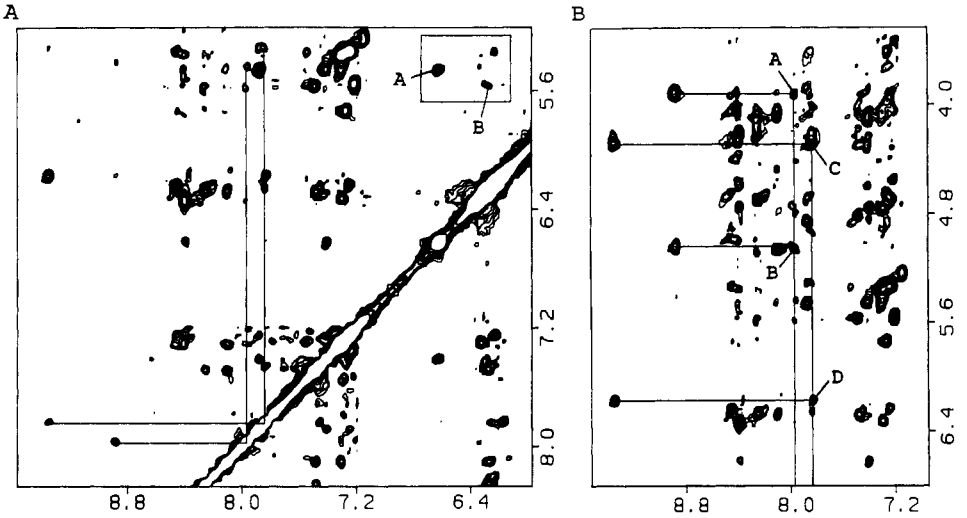

FIGURE 9: Expanded NOESY contour plots (300-ms mixing time) establishing distance connectivities in the MC-X 6-mer complex in D_2O buffer, pH 6.9, 5 °C. (A) NOE cross peaks between the 6.0–9.6 ppm and 5.2–8.2 ppm regions. The cross peaks A and B are assigned as follows: A, G10(H1′)–T11(H1′) and B, G4(H1′)–T5(H1′). (B) NOE cross peaks between the 7.0–9.6 ppm and 3.8–6.8 ppm regions. Cross peaks A–D are assigned as follows: A, MX(H10″A)–A2(H2); B, MX(H10″B)–A2(H2); C, MX(H2″)–A8(H2); D, MX(H1″)–A8(H2).

Table III: Nonexchangeable Proton Chemical Shifts in the MC-X 6-mer Complex in 0.1 M NaCl, 10 mM Phosphate, and D_2O, pH 6.9

	chemical shifts (ppm), 5 °C						
base	H8	H6	H2	H5/CH_3	H1′	H2′,2″	H3′
T1		7.21		1.49	5.56	1.48, 1.91	4.55
A2	8.40		7.96		6.32	2.88, 3.00	4.99
C3		7.30		5.35	5.44	1.66, 1.97	4.76
G4	8.10				6.28	2.91, 2.74	5.07
T5		7.48		1.81	5.58	2.08, 2.17	4.81
A6	8.25		7.46		6.27	2.65, 2.52	4.70
T7		7.27		1.50	5.74	1.74, 2.10	4.64
A8	8.45		7.83		6.24	2.87, 2.87	4.99
C9		7.24		5.37	5.31	1.50, 1.50	4.60
G10	7.87				5.46	2.72, 2.61	4.85
T11		7.41		1.66	6.62	2.10, 2.61	4.76
A12	8.39		7.31		6.35	2.65, 2.65	4.73
	chemical shifts (ppm), 20 °C						
base	H8	H6	H2	H5/CH_3	H1′	H2′,2″	H3′
T1		7.22		1.52	5.63	1.50, 1.96	4.56
A2	8.40		7.97		6.33	2.88, 3.00	5.00
C3		7.31		5.40	5.48	1.66, 2.02	4.77
G4	8.10				6.31	2.91, 2.75	5.08
T5		7.43		1.82	5.72	2.07, 2.20	4.81
A6	8.27		*a*		6.28	2.70, 2.54	4.72
T7		7.27		1.54	5.70	1.71, 2.10	4.63
A8	8.44		*a*		6.22	2.84, 2.84	4.98
C9		7.26		5.40	5.31	1.52, 1.63	4.69
G10	7.87				5.51	2.70, 2.62	4.87
T11		7.37		1.67	6.55	2.08, 2.59	4.75
A12	8.38		7.56		6.37	2.66, 2.66	4.75

[a] The A–H2 protons resonate at 7.84 and 7.86 ppm.

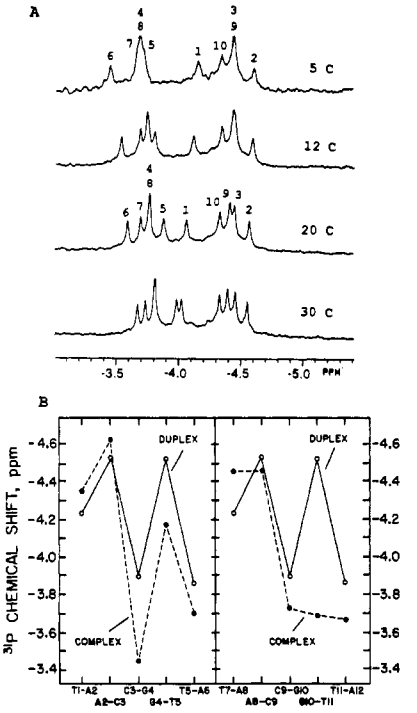

FIGURE 10: (A) Phosphorus NMR spectra (−3.0 to −5.0 ppm) of the MC-X 6-mer complex in D_2O buffer, pH 6.9, at 5, 12, 20, and 30 °C. (B) Plots of ^{31}P chemical shift versus position in the sequence for the 6-mer duplex (O) and the MC-X 6-mer complex (●). The d(T1-A2-C3-G4-T5-A6) strand is plotted on the left, and the d-(T7-A8-C9-G10-T11-A12) strand is plotted on the right.

the MC-X 6-mer complex at 30 °C are also listed in Table III.

The temperature dependence of the nonexchangeable base and sugar H1′ proton chemical shifts (6.0–8.6 ppm) of the MC-X 6-mer complex in D_2O buffer, pH 6.9, between 8 and 30 °C, exhibits several pronounced chemical shift changes with temperature (Figure 3B). The H2 proton of A6 shifts downfield (labeled with an asterisk in Figure 3B) while the H1′ of T11 shifts upfield (labeled with a double asterisk in Figure 3B) with increasing temperature.

Phosphorus Resonances in Complex. The proton-decoupled phosphorus spectra of the MC-X 6-mer complex in D_2O buffer between 5 and 30 °C are recorded in Figure 10A. Five of the ten phosphates resonate downfield of the −3.9 to −4.5 ppm region in the 5 °C spectrum (Figure 10A). The phosphorus resonances have been correlated with their three bond-coupled H3′ and H5′,5″ sugar protons and four bond-coupled H4′ sugar protons by recording proton-detected phosphorus–proton heteronuclear COSY spectra on the MC-X 6-mer complex at 5 (Figure 11A) and 20 °C (Figure 11B). Data have been recorded both in nonselective (top contour plots, Figure 11) and in H3′–P selective (bottom contour plots, Figure 11) heteronuclear COSY experiments at both temperatures.

Ten cross peaks are observed corresponding to the H3′–P coupling connectivities in nonselective proton–phosphorus correlation experiments in the MC-X 6-mer complex in D_2O at 5 (top plot, Figure 11A) and 20 °C (top plot, Figure 11B).

Table IV: Distance Constraints between Nucleic Acid Protons on Adjacent Nucleotides in the MC-X 6-mer Complex at 5 °C

	interproton distance (Å)		
	exptl	MX1	MX2
base(NH)–base(NH)			
G4(N1H)–G10(N1H)	<4.5	2.59	2.80
G4(N2H)–G10(N2H)*	<5.0	3.66	3.84
G4(N1H)–G10(N2H)	<5.0	3.56	4.17
G4(N2H)–G10(N1H)	<5.0	3.47	3.24
base(NH)–base(CH)			
G4(N1H)–A8(H2)	<5.0	3.14	3.35
G4(N2H)–A8(H2)	<4.5	3.66	3.01
G10(N1H)–A2(H2)	<5.0	4.36	3.28
G10(N2H)–A2(H2)*	<4.5	3.66	3.72
base(CH)–base(CH)			
G4(H8)–T5(CH_3)*	<3.5	2.72	3.90
G10(H8)–T11(CH_3)*	<3.5	2.71	4.51
A2(H8)–C3(H5)*	<4.0	3.15	3.83
A8(H8)–C9(H5)*	<4.0	3.67	3.72
C3(H5)–G4(H8)	>4.5	7.08	6.31
C9(H5)–G10(H8)	>4.5	8.06	7.03
A6(H2)–A8(H2)	<4.0	4.70	4.36
A2(H2)–A12(H2)	>4.5	5.56	7.21
base(CH)–sugar(CH)			
A2(H8)–T1(H1′)*	>4.5	6.21	4.65
C3(H6)–A2(H1′)	<4.0	3.22	2.68
G4(H8)–C3(H1′)*	>4.5	4.47	5.47
T5(H6)–G4(H1′)	<4.0	3.03	3.40
A6(H8)–T5(H1′)*	<4.5	3.13	2.43
A8(H8)–T7(H1′)*	>4.5	4.79	6.73
C9(H6)–A8(H1′)	<4.0	2.50	2.78
G10(H8)–C9(H1′)*	>4.5	5.14	4.85
T11(H6)–G10(H1′)	<4.0	4.68	3.35
A12(H8)–T11(H1′)*	<4.5	4.53	4.27
G4(H8)–C3(H2″)*	<4.5	2.28	3.25
G10(H8)–C9(H2″)*	<4.5	4.00	2.72
sugar(CH)–sugar(CH)			
T1(H1′)–A2(H1′)	>4.5	7.56	4.39
A2(H1′)–C3(H1′)	>4.5	3.25	4.86
C3(H1′)–G4(H1′)	>4.5	6.24	6.25
G4(H1′)–T5(H1′)	<4.5	3.84	3.41
T5(H1′)–A6(H1′)	>4.5	4.97	4.80
T7(H1′)–A8(H1′)	>4.5	5.57	6.67
A8(H1′)–C9(H1′)	>4.5	5.08	3.98
C9(H1′)–G10(H1′)	>4.5	5.98	5.80
G10(H1′)–T11(H1′)	<4.0	4.30	4.06
T11(H1′)–A12(H1′)	>4.5	5.78	6.13

Table V: Distance Constraints between Mitomycin and Nucleic Acid Protons in the MC-X 6-mer Complex at 5 °C

	interproton distance (Å)		
	exptl	MX1	MX2
base(NH)–mitomycin(CH)			
G4(N2H)–MC(H1″)	<4.5	3.07	3.05
G4(N2H)–MC(H2″)*	<4.0	2.48	3.12
G10(N2H)–MC(H10″A)	<4.0	2.50	2.74
G10(N2H)–MC(H10″B)	<4.0	2.41	2.24
G4(N2H)–MC(H10″A)*	>4.5	4.43	5.07
G4(N2H)–MC(H10″B)*	>4.5	3.58	4.36
G10(N2H)–MC(H1″)*	>4.5	4.89	3.72
G10(N2H)–MC(H2″)	>4.5	5.88	6.00
base(CH)–mitomycin(CH)			
A8(H2)–MC(H1″)*	<4.0	4.01	4.24
A8(H2)–MC(H2″)*	<4.0	4.17	2.34
A2(H2)–MC(H10″A)	<4.5	4.03	5.60
A2(H2)–MC(H10″B)	<4.5	5.33	5.80
A8(H2)–MC(H10″A)	>4.5	7.48	7.75
A8(H2)–MC(H10″B)	>4.5	6.00	6.64
A2(H2)–MC(H1″)	>4.5	8.20	7.30
A2(H2)–MC(H2″)	>4.5	8.63	9.25

The phosphorus resonances have been assigned from a knowledge of the sugar H3′ assignments, and these phosphorus assignments are listed in Table II and plotted in Figure 10B. The assignments were aided by the observed shifts in both backbone phosphates and sugar H3′ protons between 5 and 20 °C so that chemical shifts which are overlapped at one temperature were resolved at the other. The six phosphorus resonances in the (C3-G4-T5-A6)·(C9-G10-T11-A12) segment of the MC-X 6-mer complex resonate at low field with several of these exhibiting pronounced temperature-dependent chemical shifts (Figure 10A).

The corresponding H3′–P coupling connectivities in selective proton–phosphorus correlation experiments have also been assigned in the MC-X 6-mer complex plot at 5 (bottom plot, Figure 11A) and 20 °C (bottom plot, Figure 11B). It should be noted that cross peak 4 (assigned to G10-T11) exhibits a distinct pattern in the nonselective experiment (top contour plots, Figure 11A,B), indicative of an ususually large phosphorus–sugar proton coupling constant(s) at the G10-T11 linkage. This cannot reflect a large H3′–P coupling constant at G10-T11 because cross peak 4 exhibits a normal pattern similar to those of the remaining cross peaks in the selective H3′–P heteronuclear COSY experiments (bottom contour plots, Figure 11A,B). Thus, the unusually large heteronuclear coupling constant at G10-T11 must originate in either the three bond P–H5′/H5″ and/or four bond P–H4′ coupling connectivities.

NMR Distance Constraints in Complex. The proton–proton distance constraints in the MC-X 6-mer complex can be subdivided into those between nucleic acid protons (Table IV) and those between mitomycin and nucleic acid protons (Table V). Upper distance limits are listed for those distances defined by observable NOE cross peaks with the relative magnitude of the limit defined by the relative intensity of the cross peak. In addition, a lower distance limit is also defined for a select set of proton–proton distances that do not exhibit an observable NOE cross peak in the NOESY contour plot of the MC-X 6-mer complex.

The alignment of G4·C9 and C3·G10 pairs at the cross-link site is defined by a set of NOEs between the imino and amino protons of G4 and G10 in the MC-X 6-mer complex (Table IV). Further, NOEs are detected between these deoxyguanosine exchangeable protons in G·C pairs and the deoxyadenosine H2 protons on adjacent A·T pairs in the (A2-C3-G4-T5)·(A8-C9-G10-T11) segment of the MC-X 6-mer complex (Table IV). A set of base H8–base H5/CH_3 NOEs puts constraints on the stacking alignment at purine(3′–5′)-pyrimidine steps in the MC-X 6-mer (Table IV). Differences are detected for the observed NOEs between H2 protons of deoxyadenosines on adjacent pairs at either end of the helix with the stronger NOE detected for the (T5-A6)·(T7-A8) step relative to the (T1-A2)·(T11-A12) step (Table IV).

The perturbation in the DNA conformation can be monitored by the relative strength of the NOE between base (purine H8 or pyrimidine H6) and the sugar H1′ protons of the 5′-flanking residue. These constraints are listed in Table IV for the MC-X 6-mer complex and exhibit an alternating pattern of observed NOEs at purine–pyrimidine steps and very weak or absent NOEs at pyrimidine–purine steps. A pair of unexpected constraints was detected between the sugar H1′ protons on adjacent residues at the G4-T5 and G10-T11 steps, and hence upper bounds were assigned at these positions. Lower bounds consistent with the absence of NOEs between adjacent sugar H1′ protons at the remaining steps in the MC-X 6-mer complex are also included in Table IV.

The cross-link site is defined by a set of NOE constraints between the amino proton of G4 and the H1″, H2″ protons

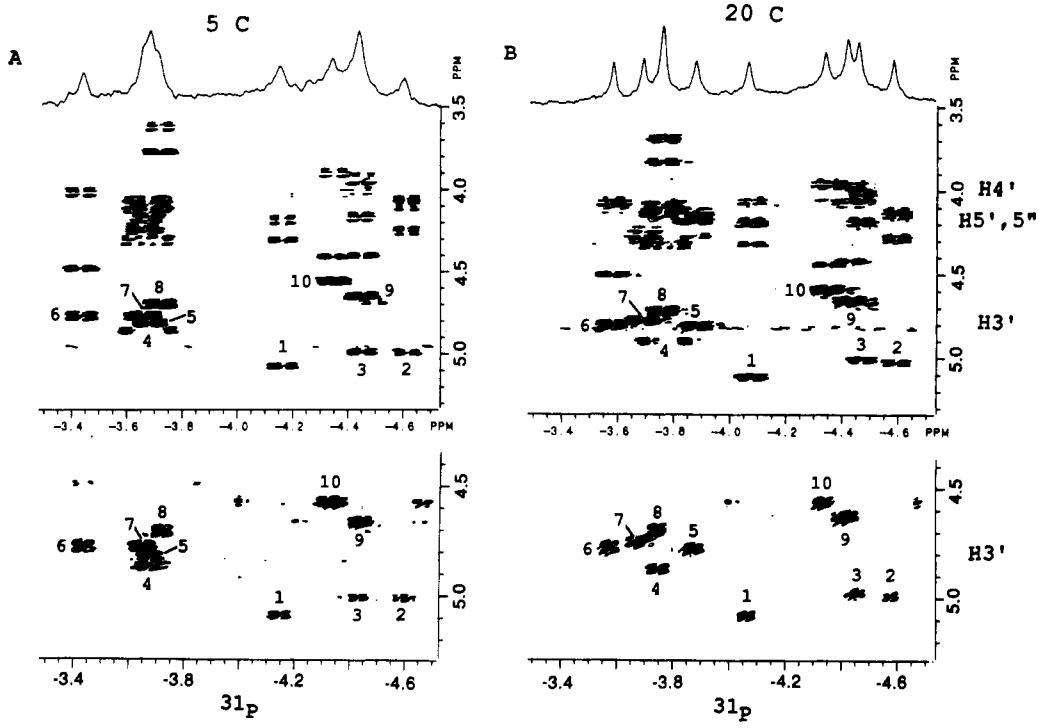

FIGURE 11: Contour plots of the proton-detected phosphorus–proton heteronuclear COSY experiment on the MC-X 6-mer complex in D_2O buffer, pH 6.9, at (A) 5 and (B) 20 °C. The phosphorus dimension extends from −3.4 to −4.7 ppm with the one-dimensional phosphorus spectrum recorded over the contour plot. The proton dimension extends from 3.5 to 5.2 ppm and encompasses the sugar H4′, H5′,H5″ protons (3.5–4.5 ppm) and the sugar H3′ protons (4.5–5.1 ppm). The top plots in (A) and (B) are nonselective experiments, and the bottom plots in (A) and (B) correspond to a selective ^{31}P–H3′ experiment.

of mitomycin and another set of NOEs between the amino proton of G10 and the geminal H10″ protons of mitomycin in the MC-X 6-mer complex (Table V). Additional constraints are available between these mitomycin protons and the H2 protons on the A2·T11 and T5·A8 base pairs that flank the cross-link site (Table V).

Minimized Potential Energy Computations on Complex. Conformation space searches (methodology outlined under Experimental Procedures) on the MC-X 6-mer complex were guided by the distance constraints (marked by asterisks) listed in Tables IV and V that define structural elements of the cross-link site and identify those regions of the duplex DNA that are distorted on complex formation. The minimizations were undertaken on the MC-X 6-mer complex starting from the DNA in the B-helical fiber diffraction model (Arnott et al., 1976) with the torsion angles associated with mitomycin and the linkage site chosen from preliminary model building ($\alpha' = 0°$, $\beta' = 270°$, $\gamma' = 300°$, $\delta' = 45°$, $\epsilon' = 180°$, $\alpha'' = 0°$, and $\beta'' = 60°$). The mitomycin nonplanar five-membered ring pucker was kept fixed during the minimizations in either conformer M1 (mitomycin C2″ is puckered in the same direction as the N2 of deoxyguanosine linked to C1″) or conformer M2 (pucker is in the opposite direction). The constraints included the hydrogen-bond forcing function at all base pairs except the terminal A·T pairs together with the distance constraints indicated by asterisks in Tables IV and V using eqs 1 and 2 (supplementary material). All constraints were removed in the final minimization stages.

A stereoview of the nonterminal segment of the final unconstrained energy-minimized conformation MX1 of the MC-X 6-mer complex starting from the fixed M1 pucker of the mitomycin saturated five-membered ring is shown in stereo in Figure 12A. The corresponding final unconstrained energy minimized conformation MX2 starting from the fixed M2 pucker of the mitomycin saturated five-membered ring is shown in stereo in Figure 12B. Alternate stereoviews of the central cross-linked dinucleotide segment of the MC-X 6-mer complex emphasizing the covalent bonds between mitomycin and the DNA are drawn for conformer MX1 in Figure S1A and for conformer MX2 in Figure S1B (see supplementary material). The backbone torsion angles in the (A2-C3-G4-T5)·(A8-C9-G10-T11) segment of the MC-X 6-mer complex conformations MX1 and MX2 are listed in Table VI.

The stereoviews of MX1 and MX2 focus on the central tetranucleotide segment in Figure 12 since NMR experiments rule out pairing at the terminal A·T pairs. In the absence of this constraint no unique structure defines the conformation at either end of the helix.

Interproton Distances in Conformations MX1 and MX2. The experimental distance constraints include NOEs between nucleic acid protons on adjacent nucleotides (Table IV) and NOEs between mitomycin and nucleic acid protons (Table V) in the MC-X 6-mer complex at 5 °C. These constraints are defined as either a lower or an upper bound. This reflects the nature of the experimental data which are based on one-dimensional NOE experiments on the complex in H_2O and on a 300-ms mixing time NOESY data set on the complex in D_2O solution.

The interproton distances in conformations MX1 and MX2 can be compared to the corresponding experimental distance constraints for the MC-X 6-mer complex in Tables IV and V. The majority of the distances in conformations MX1 and MX2 satisfy the experimental distance constraints. A few distances in MX1 and MX2 are <1 Å outside the experimental distance limits, and a very few distances between base and 5′-sugar H1′ protons range between 2.5 and 2.8 Å, a short distance that would result in a stronger NOE than observed experimentally.

Discussion

Fraying at the Ends of the d(T-A-C-G-T-A) Duplex. The imino proton of terminal T1 resonates at 11.12 ppm in the

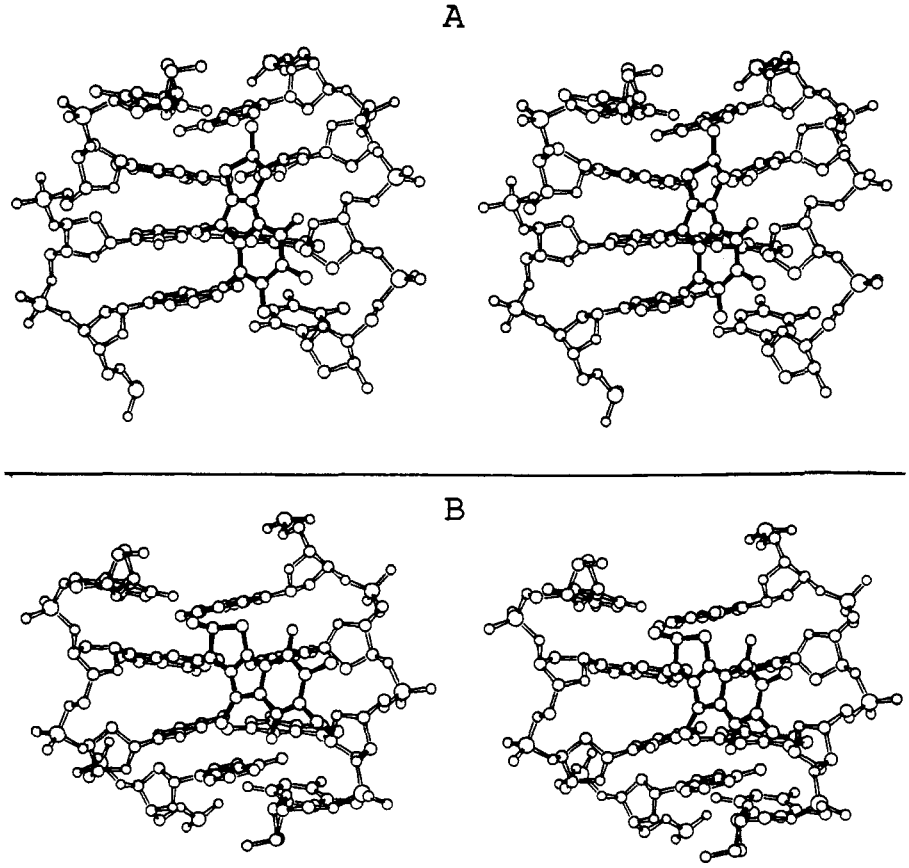

FIGURE 12: Stereoviews of the (A2-C3-G4-T5)·(A8-C9-G10-T11) tetranucleotide segment of the fully unconstrained energy-minimized (A) MX1 conformation and (B) MX2 conformation of the MC-X 6-mer complex. The mitomycin ring system is drawn with dark bonds and is cross-linked in the minor groove. The strand on the left corresponds to A2-C3-G4-T5 running from bottom to top, while the strand on the right corresponds to A8-C9-G10-T11 running from top to bottom in the stereoview of the MX1 and MX2 conformations of the MC-X 6-mer complex.

d(T-A-C-G-T-A) duplex which is to high field of the thymidine imino protons in Watson–Crick A·T pairs (13.5–14.5 ppm). Further, the NOE between the imino proton of T1 and the H2 proton of A6 is barely detectable for the d(T-A-C-G-T-A) duplex (Figure 1D). These observations suggest that the terminal T1 is either weakly paired or unpaired to A6 in the d(T1-A2-C3-G4-T5-A6) duplex at low temperature. This conclusion is supported by the observed NOEs between base protons and their 5′-flanking sugar H1′ protons which are much weaker at the T1-A2 and T5-A6 steps relative to all other steps in the d(T-A-C-G-T-A) duplex. By contrast, the chemical shift and NOE data establish that the terminal A1·T6 base pairs are stable in the related self-complementary d(A1-T2-G3-C4-A5-T6) duplex at low temperature (Patel, 1974). Thus, the pairing of terminal A·T pairs in DNA duplexes appears to depend on whether the terminal step is 5′-T-A-3′ or 5′-A-T-3′ at the ends of the helix.

There also appear to be distinct differences in the phosphate backbone between pyrimidine–purine (T1-A2, C3-G4 and T5-A6) steps and purine–pyrimidine (A2-C3 and G4-T5) steps in the d(T-A-C-G-T-A) duplex since a sinusoidal pattern is observed in the phosphorus chemical shifts with the former internucleotide phosphates resonating downfield of the latter internucleotide phosphates (Figure 10B, open circles). Previous workers have attempted to correlate such phosphorus chemical shift variations with changes in sequence-dependent helical parameters (Gorenstein et al., 1988).

Mitomycin·d(T-A-C-G-T-A) Complex. The exchangeable and nonexchangeable proton spectra of the MC-X 6-mer complex as a function of temperature are plotted in parts A and B of Figure 3, respectively. We detect resonances originating from a minor adduct in slow exchange with the major cross-linked complex. We were unable to separate the minor and major adducts by HPLC, and the present studies have focused on the major cross-linked MC-X 6-mer complex.

Minor Groove Linkage. The NMR studies readily establish that mitomycin cross-linking occurs to the minor groove guanosine 2-amino position of G4 and G10 in the d(T-A-C-G-T-A) duplex. Further, the cross-linking occurs through the side chain C10″ and the ring-opened aziridine C1″ position on the mitomycin ring. These conclusions are based on the NOE (Figure 5A) and coupling (Figure 5B) connectivities between the G10 amino proton and the geminal H10″A, H10″B mitomycin protons (peaks C and D, Figure 5A,B) [establishes G10(N2)–MC(C10″) linkage] and connectivities between the G4 amino proton and the H1′ mitomycin proton (peak A, Figure 5A,B) [establishes G4(N2)–MC(C1″) linkage] in the MC-X 6-mer complex.

Further support for positioning mitomycin in the minor groove is based on the observed NOEs between mitomycin H1″, H2″ protons and the minor groove H2 proton of A8 (peaks C and D, Figure 9B) and NOEs between the mitomycin H10″A, H10″B protons and the minor groove H2 proton of A2 (peaks A and B, Figure 9B) in the MC-X 6-mer complex.

G·C Pairing. The exchangeable proton NMR spectra establish the integrity and pairing alignment of the G4·C9 and C3·G10 base pairs of the mitomycin cross-link site in the MC-X 6-mer complex. The observed NOEs between the deoxyguanosine imino proton and the amino protons of deoxyguanosine and deoxycytidine establish Watson–Crick pairing at both G4·C9 (Figure 4B) and C3·G10 (Figure 4C) base pairs. The imino protons of G4 (13.12 ppm) and G10

Table VI: Backbone Torsion Angles for the (A2-C3-G4-T5)·(A8-C9-G10-T11) Segment in the Energy-Minimized MX1 and MX2 Conformations of the MC-X 6-mer Complex[a]

	α	β	γ	P	χ	ϵ	ζ
				MX1 Conformer[b]			
A2	275	163	48	165	299	194	277
C3	252	66	172	170	221	185	259
G4	235	235	69	176	287	187	216
T5	312	137	66	151	245	178	262
A8	302	177	64	171	247	189	232
C9	305	173	50	163	226	199	275
G10	314	250	307	311	272	189	294
T11	273	171	55	29	252	189	283
				MX2 Conformer[c]			
A2	296	157	75	167	261	192	216
C3	298	157	60	152	233	219	272
G4	278	181	36	157	296	199	191
T5	308	110	81	154	242	185	242
A8	300	224	64	177	302	201	197
C9	305	126	62	78	230	189	252
G10	291	177	65	182	265	188	251
T11	278	157	80	130	238	188	263

[a] Torsion angle definitions associated with the mitomycin and the mitomycin–DNA linkage site are as follows: α', N1G–C2G–N2G–C1″; β', C2G–N2G–C1″–C2″; β'', C1″–C2″–N2″–H2″A; α'', C5″–C6″–C6A″–H6A″; γ', C8A″–C9″–C10″–N2G; δ', C9″–C10″–N2G–C2G; ϵ', C10″–N2G–C2G–N1G. For the DNA, the torsion angle definitions are χ(pyr), O1′–C1′–N1–C2; χ(pur), O1′–C1′–N9–C4; ϵ, P–O3′–C3′–C4′; ζ, O5′–P–O3′–C3′; α, C5′–O5′–P–O3′; β, C4′–C5′–O5′–P; and γ, C3′–C4′–C5′–O5′. The angle A–B–C–D is measured by a clockwise rotation of D with respect to A looking down the B–C bond. A eclipsing D is 0°. Sugar pucker is determined by the pseudorotation parameter P (Altona & Sundaralingam, 1972). [b] α' = 162, β' = 221, γ' = 260, δ' = 18, and ϵ' = 193. [c] α' = 187, β' = 260, γ' = 253, δ' = 45, and ϵ' = 207.

(12.60 ppm) resonate in the spectral region characteristic of Watson–Crick G·C pairs but exhibit a 0.48 ppm separation in MC-X 6-mer complex for sequence symmetry related positions.

Previous studies have established that deoxyguanosine amino protons exhibit broad spectra at room temperature due to intermediate rotation rates about the C–NH_2 bond (Patel, 1976). For the MC-X 6-mer complex there is only a single amino proton at each deoxyguanosine (Figure 3A) with a fixed C–N bond torsion angle due to the presence of the cross-link. Therefore, the observation of narrow deoxyguanosine amino protons for G4 (9.36 ppm) and G10 (8.87 ppm) were not unexpected, but it was of interest to note that both deoxyguanosine amino protons resonate to low field of the hydrogen-bonded deoxycytidine amino protons of C3 (8.33 ppm) and C9 (8.15 ppm) (Figure 3A). These downfield shifts suggest that the deoxyguanosine amino protons form strong hydrogen bonds to the carbonyl groups of deoxycytidine for both G4·C9 and C3·G10 base pairs. This conclusion is supported by the slow exchange of the deoxyguanosine amino protons when the MC-X 6-mer complex is transferred from H_2O to D_2O solution. The 0.49 ppm separation of the sequence symmetry related amino protons of G4 and G10 matches the corresponding separation for the imino protons at these positions in the MC-X 6-mer complex.

A·T Pairing. The NMR parameters of the thymidine imino protons of the internal A2·T11 and T5·A8 base pairs exhibit distinct differences from those observed for the T1·A12 and A6·T7 base pairs in the MC-X 6-mer complex. The observed medium-intensity NOEs between the T5 imino proton and the H2 proton of A8 (Figure 4F) and between the T11 imino proton and the H2 proton of A2 (Figure 4G) establish formation of standard Watson–Crick A2·T11 and T5·A8 base pairs adjacent to the cross-link site. Further, the imino proton chemical shifts of T5 (13.45 ppm) and T11 (13.19 ppm) in the MC-X 6-mer complex (Table II) are shifted upfield relative to their chemical shift (14.06 ppm) in the free duplex (Table I). Such large upfield shifts could reflect either that there is increased stacking due to changes in base pair overlaps and/or that hydrogen bonding is somewhat weakened at the A2·T11 base pair and to a lesser extent at the T5·A8 base pair on complex formation.

By contrast, the imino protons of T1 (10.86 ppm) and T7 (11.48 ppm) resonate to higher field (Figure 3A) and exhibit chemical shifts characteristic of either weakly paired or unpaired thymidines. Further, associated with these upfield shifts are very weak NOEs between the T7 imino proton and the H2 proton of A6 (Figure 4H) and between the T1 imino proton and the H2 proton of A12 (Figure 4I).

Thus, we detect parallel structural features for the d(T-A-C-G-T-A) duplex and its mitomycin cross-link in that the internal A·T and G·C pairs are stabilized by Watson–Crick hydrogen bonding while there is either weak pairing or disruption of the terminal A·T pairs.

The temperature dependence of the exchangeable proton spectra of the MC-X 6-mer complex establishes that all the thymidine imino protons broaden and shift upfield when the temperature is raised from −1 to 24 °C, while the imino and amino protons of G4 and G10 at the cross-link site neither shift nor broaden in this temperature range (Figure 3A). Thus, the cross-linked (C3-G4)·(C9-G10) central segment of the duplex forms a stable core in the MC-X 6-mer complex.

Base Pair Stacking. The observed NOEs between thymidine imino, deoxyguanosine imino, deoxyguanosine amino, and deoxyadenosine H2 protons on adjacent base pairs establish base pair stacking in the nonterminal (A2-C3-G4-T5)·(A8-C9-G10-T11) segment of the MC-X 6-mer complex. This stacking is readily demonstrated for adjacent G4·C9 and C3·G10 base pairs at the cross-link site and is defined by NOEs between the imino protons of G4 and G10 (Figure 4B,C), NOEs between the imino proton of G4 and the amino proton of G10 (Figure 4D), and NOEs between the imino proton of G10 and the amino proton of G4 (Figure 4E), as well as weak NOEs between the amino protons of G4 and G10 (Figure 4D,E). These results establish maintenance of base pair stacking centered about the mitomycin cross-link site in the MC-X 6-mer complex.

Base stacking of the A2·T11 and C3·G10 base pairs is reflected in the observed NOEs between the imino protons of T11 and G10 (Figure 4G), while base stacking of G4·C9 and T5·A8 base pairs is reflected in the observed NOEs between the imino protons of G4 and T5 (Figure 4F) in the MC-X 6-mer complex.

Structural Perturbations. We observe distinct differences in the NOE connectivities for pyrimidine–purine and purine–pyrimidine steps in the MC-X 6-mer complex. The NOE connectivities are characteristic of unperturbed helical segments at the A2-C3, G4-T5, A8-C9, and G10-T11 purine-(3′–5′)pyrimidine steps. Thus, base–sugar NOEs are detected between the pyrimidine H6 proton and its 5′-linked purine sugar protons (Figure 7), and base–base NOEs are detected between purine H8 and pyrimidine H5/CH_3 protons (Figures 6B and 7), characteristic of regular right-handed duplex segments. By contrast, the base–sugar NOEs are either weak or absent between the purine H8 and its 5′-linked pyrimidine sugar H1′ protons in the T1-A2, C3-G4, T5-A6, T7-A8, C9-G10, and T11-A12 pyrimidine(3′–5′)purine steps (Figure 7). It is important to note that an NOE was detected between

the H8 proton of deoxyguanosine and the H1′ proton of deoxycytidine in the central C-G step in the 6-mer duplex (Figure 2A) but is missing for the same steps on both strands in the MC-X 6-mer complex (Figure 7A,B).

Sugar protons on adjacent residues are >5 Å apart in regular DNA helices, and hence NOEs are not detected between sugar H1′ protons on adjacent residues. However, an NOE is detected between the sugar H1′ protons of G10 and T11 (peak A, Figure 9A), and a weaker NOE is detected between the sugar H1′ protons of G4 and T5 (peak B, Figure 9A) in the MC-X 6-mer complex. Thus, mitomycin cross-link formation is accommodated, in part, by a perturbation in the backbone of the G10-T11 step and to a lesser extent in the G4-T5 step which brings the sugar rings at these positions into close proximity.

(C3-G4-T5)·(C9-G10-T11) Segment. Several large nonexchangeable proton complexation shifts are detected following comparison of the chemical shifts in the 6-mer duplex at 10 °C (Table I) and in the MC-X 6-mer complex at 5 °C (Table III) with upfield shifts observed for the H1′ proton of G10 (0.44 ppm) and the H2″ proton of C9 (0.89 ppm) and downfield shifts observed for the H1′ proton of T11 (0.78 ppm) and the H2″ proton of T11 (0.51 ppm). Further, large shift differences are detected between sequence symmetry related positions as detected for the H1′ protons of G4/G10 (0.82 ppm), H1′ protons of T5/T11 (1.04 ppm), H2″ protons of C3/C9 (0.47 ppm), and H2″ protons of T5/T11 (0.44 ppm) in the complex. These results demonstrate that complex formation results in large sugar proton chemical shift differences at the minor groove H1′ and H2″ protons of the C9-G10-T11 segment on one strand and that the major difference in parameters between the two strands in the complex is localized to the sequence symmetry related C3-G4-T5 and C9-G10-T11 segments centered about the cross-link site.

The chemical shift differences for phosphorus resonances between the 6-mer duplex at 5 °C and the MC-X 6-mer complex at 5 °C can be readily visualized in the plots drawn in Figure 10B. The phosphorus resonances in the pyrimidine–purine (T1-A2, C3-G4, and T5-A6) steps resonate upfield (by up to 0.6 ppm) from their counterparts in purine–pyrimidine (A2-C3 and G4-T5) steps in the 6-mer duplex. This sinusoidal pattern is maintained for the phosphorus chemical shifts in the T1-A2-C3-G4-T5-A6 strand (left panel, Figure 10B) but breaks down at the G10-T11 step for the phosphorus chemical shifts in the T7-A8-C9-G10-T11-A12 strand (right panel, Figure 10B) in the MC-X 6-mer complex.

The largest chemical shift differences associated with mitomycin cross-linking at G4 and G10 are downfield phosphorus shifts at the C3-G4 (0.45 ppm), G4-T5 (0.35 ppm), and G10-T11 (0.89 ppm) linkages (Table II; Figure 10B). The largest phosphorus chemical shift differences between phosphate linkages related by sequence symmetry are observed at the C3-G4/C9-G10 steps (0.28 ppm) and at the G4-T5/G10-T11 steps (0.49 ppm) in the MC-X 6-mer complex (Table II; Figure 10B). Thus, complex formation results in the largest perturbation in the phosphate backbone at the G10-T11 step, and, further, the largest difference between the partner strands occurs between the C3-G4-T5 segment and its sequence symmetry related C9-G10-T11 segment.

Mitomycin Alignment in the Minor Groove. The alignment of the mitomycin in the minor groove can be inferred from the NMR parameters for the MC-X 6-mer complex at 5 °C. Specifically, the H1′ proton of G10 (5.46 ppm) resonates to high field of all the purine H1′ protons including G4 (6.28 ppm), its sequence symmetry related partner, while the H1′ proton of T11 (6.62 ppm) resonates to low field of all the pyrimidine H1′ protons including T5 (5.58 ppm), its sequence symmetry related partner (Table III; Figure 7). The unusual upfield shift of the H1′ proton of G10 and the unusual downfield shift of the H1′ proton of T11 establishes that the mitomycin aromatic chromophore is aligned toward the G10-T11 step of the T7-A8-C9-G10-T11-A12 strand rather than positioned in the center of the minor groove of the MC-X 6-mer complex.

The experimental chemical shift data further predict that the H1′ proton of G10 will be positioned over the plane of the mitomycin chromophore (upfield ring current shifts) while the H1′ proton of T11 will be positioned approximately in the plane of the mitomycin chromophore (downfield ring current shifts) in the MC-X 6-mer complex.

MX1 and MX2 Conformations. We employed two different starting fixed puckers of the nonplanar five-membered ring of mitomycin, and these remained rigid during energy minimization studies on the complex. This procedure is consistent with the linked atom algorithm, which employs fixed bond lengths, bond angles, and dihedral angles, while permitting movements in those nonring torsion angles about which large conformational rearrangements occur (sugar puckers are, however, flexible in our algorithm). Treatment of the mitomycin nonplanar five-membered ring conformation as two alternate rigid structures that are energy minima is a reasonable approximation suitable for our computational approach.

The MX1 and MX2 conformations defined by the torsion angles listed in Table VI are fully unconstrained minimum energy conformations that are within (or close to) the experimental distance constraints listed in Tables IV and V. The distance constraints designated by asterisks in Tables IV and V and the hydrogen bond forcing function (supplementary material) are employed in the initial minimization stages only as devices for guiding the minimizer in the search for energy minima that are consistent with measured results. Our attempts at using all the experimental distance constraints listed in Tables IV and V were less successful in finding suitable conformations probably due to the increased number of variables, which further taxes the optimization algorithm.

In the final minimizations all constraints are released. It is noteworthy that the interproton distances for the computed MX1 and MX2 conformations of the complex are within the ranges (or in a few cases approach the ranges) of all the distance constraints of Tables IV and V, while only the experimental distances designated by asterisks were actually constrained in the calculations.

The backbone torsion angles of the DNA and the torsion angles at the linkage site of mitomycin to DNA for the MX1 and MX2 conformations of the complex are summarized in Table VI. The torsion angles defining the cross-link site **2** are similar for the MX1 and MX2 conformations (Table VI), indicative of a preferred linkage alignment for mitomycin to deoxyguanosine N2 positions on adjacent G·C pairs in the (C-G)·(C-G) step.

Sequence-dependent variations in the width of the minor groove of B-form DNA range between 3 and 7 Å in a crystal of a B-DNA dodecanucleotide duplex (Dickerson et al., 1982). We find that the minor groove widens to an average of 10.8 Å in MX1 and 9.2 Å in MX2 on formation of the mitomycin cross-link for the computed MC-X 6-mer complex conformations.

Several DNA backbone torsion angles in the MX1 conformation differ from the range of values observed for B_1 form structures in a dodecanucleotide crystal (Drew et al., 1981). The largest differences are observed at the β and γ torsion angles for C3 and the γ torsion angle for G10 (Table VI). By contrast, the backbone torsion angles in the MX2 conformation deviate to a lesser degree from the range of values observed for B-DNA in the crystalline state (Table VI).

Several sugar puckers defined by the pseudorotation parameter **P** deviate from the C2′-endo (centered at **P** = 180°) in both the MX1 (sugars G10 and T11) and the MX2 (sugar C9) conformations (Table VI). Similarly, glycosidic torsion angles in the high anti range ($\chi \sim 300°$) are detected in both the MX1 (residues A2 and G4) and the MX2 (residues G4 and A8) conformations (Table VI).

An effort was made to place the mitomycin M2 conformer in the DNA site accommodating the M1 conformer in the MX1 conformation of the complex and similarly to place M1 in the MX2 conformation. This was done by replacing M1 with M2 (or M2 with M1) in the final unconstrained MX1 (or MX2) conformation and reminimizing, first with constraints and then without them. This approach was unsuccessful since base pair alignments became severely distorted and several interproton distances were well outside the experimental distance constraints.

Thus, our combined NMR and computational studies have determined two conformations, MX1 and MX2, for the MC-X 6-mer complex which satisfy the experimental distance constraints. Our experimental data do not permit us to select one over the other of these conformations, nor do they rule out a rapid equilibrium between MX1 and MX2 conformations for the MC-X 6-mer complex in aqueous solution.

Earlier Models of Mitomycin Cross-Link Site. The mitomycin cross-link at the (C-G)·(C-G) step has been previously computed (Verdine, 1986; Tomasz et al., 1987) without the benefit of experimental interproton distance constraints. The earlier model (Tomasz et al., 1987) and the current study agree that Watson–Crick base pairing was maintained at the (C-G)·(C-G) cross-link site, that the glycosidic bonds adopt anti rather than syn conformations, that base stacking was maintained, and that the cross-linked mitomycin is directed toward one of the strands. The DNA retains its unperturbed B conformation in the earlier model (Tomasz et al., 1987) in contrast to the structural distortions observed experimentally in this study. The nonplanar five-membered ring of mitomycin is planar in the earlier model (Tomasz et al., 1987) in contrast to the present study, which considered both pucker orientations for this ring system.

Overall, the present study, which is guided by experimental distance constraints and which more readily permits distortion to the DNA structure and enforces appropriate puckers to the saturated five-membered ring of mitomycin, improves on the earlier models of the structure of mitomycin cross-linked at (C-G)·(C-G) steps in DNA.

Summary. The solution conformation of mitomycin cross-linked to the self-complementary d(T1-A2-C3-G4-T5-A6)·d(T7-A8-C9-G10-T11-A12) duplex has been characterized by a two-dimensional NMR study of the MC-X 6-mer complex followed by energy minimization computations guided by experimental proton–proton distance constraints.

The NMR parameters establish that mitomycin cross-links in the minor groove to adjacent deoxyguanosines on partner strands at the (C3-G4)·(C9-G10) central segment in the MC-X 6-mer complex. The cross-link involves G4(N2)–MC(C1″) and G10(N2)–MC(C10″) covalent linkages without disruption of the C3·G10 and G4·C9 Watson–Crick pairs. Further, the observed NOEs between the mitomycin H1″, H2″ protons and the deoxyadenosine H2 proton of the T5·A8 base pair and between the mitomycin geminal H10″ protons and the deoxyadenosine H2 proton of the A2·T11 base pair put additional constraints on mitomycin alignment in the minor groove.

The proton NMR parameters demonstrate fraying at the ends of the d(T-A-C-G-T-A) duplex, and this feature is retained on mitomycin cross-link formation. We detect similar patterns of NOEs between nucleic acid protons at symmetry-related positions on the d(T1-A2-C3-G4-T5-A6) and the d(T7-A8-C9-G10-T11-A12) strands in the MC-X 6-mer complex except that differences are detected when the G10-T11 step is compared to its symmetry-related G4-T5 step. Thus, the sugar rings of G10 and T11 are somewhat closer to each other than are the sugar rings of G4 and T5 as determined by the unusual NOE between the sugar H1′ protons on adjacent nucleotides in the MC-X 6-mer complex. Similarly, the backbone phosphate chemical shifts at the G4-T5 and G10-T11 steps are separated by 0.49 ppm in the complex.

The observed and assigned NOEs between nucleic acid protons and between mitomycin and nucleic acid protons in NOESY data sets on the MC-X 6-mer complex in H_2O and D_2O yield a set of experimental proton–proton distance constraints with conservative allowance for error. These constraints were incorporated in minimized potential energy calculations in torsion angle space starting from a fixed nonplanar five-membered ring of mitomycin in each of two pucker (M1 and M2) orientations. The resulting minimum energy conformations MX1 and MX2 satisfy the majority of the experimental distance constraints and are characterized by a widened minor groove at the cross-link site with the mitomycin chromophore directed toward the d(T7-A8-C9-G10-T11-A12) strand in the complex. The NMR experimental data, which indicate large shifts detected at the minor groove sugar protons of C9, G10, and T11 on complex formation, support this orientation.

Conformations MX1 and MX2, which differ in the pucker of the nonplanar five-membered ring of mitomycin, exhibit similar torsion angles at the bonds involved at the covalent linkage sites but differ at some specific nucleic acid backbone torsion angles. We are currently unable to select between conformations MX1 and MX2 for the structure of the MC-X 6-mer in solution.

Acknowledgments

S.B. thanks Prof. Stephen Wilson, Chemistry Department, New York University, for generating the two mitomycin conformers M1 and M2 with the program Macromodel, Prof. Robert Shapiro, Chemistry Department, New York University, for many helpful discussions, and Suresh B. Singh, Chemistry Department, New York University, for computational assistance.

Supplementary Material Available

Full description of the procedures used in the minimized potential energy calculations in torsion angle space using the DUPLEX program, tables listing nonredundant set of bond lengths, bond angles, and dihedral angles for mitomycin and linkage site (Table A), coordinates for conformers M1 and M2 (Table B), partial charges of mitomycin and linkage site (Table C), and torsion barriers (Table D), and a figure showing a stereoview of the central cross-linked dinucleotide segment of MC-X 6-mer complex emphasizing the covalent

bonds between mitomycin and DNA (11 pages). Ordering information is given on any current masthead page.

References

Altona, C., & Sundaraligam, M. (1972) *J. Am. Chem. Soc. 94*, 8205–8212.

Arnott, S., Campbell, P., & Chandrasekharan, R. (1976) in *Handbook of Biochemistry and Molecular Biology* (Fasman, G., Ed.) CRC Press, Cleveland, OH.

Balbinder, E., & Kerry, D. (1984) *Mutat. Res. 130*, 315–320.

Borowy-Borowski, H., Lipman, R., Chowdary, D., & Tomasz, M. (1990) *Biochemistry* (in press).

Carter, S. K., & Crooke, S. T. (1979) *Mitomycin C, Current Status and New Developments*, Academic Press, New York.

Cera, C., & Crothers, D. M. (1989) *Biochemistry 28*, 3908–3911.

Chawla, A. K., Lipman, R., & Tomasz, M. (1987) in *Structure and Expression, Vol. 2. DNA and its Drug Complexes* (Sarma, R. H., & Sarma, M. H., Eds.) Adenine Press, Schenectady, NY.

Dickerson, R. E., Kopka, M., & Drew, H. (1982) in *Conformation in Biology* (Srinivasan, R., & Sarma, R. H., Eds.) pp 227–257, Adenine Press, New York.

Drew, H. R., Wing, R., Takano, T., Broka, C., Tanaka, S., Itakura, K., & Dickerson, R. E. (1981) *Proc. Natl. Acad. Sci. U.S.A. 78*, 2179–2183.

Gorenstein, D. G., Schroeder, S. A., Fu, J. M., Metz, J. T., Roongta, V., & Jones, C. R. (1988) *Biochemistry 27*, 7223–7227.

Hata, T., Sano, Y., Sugawara, R., Matsumae, A., Kanamori, K., Shima, T., & Hoshi, T. (1956) *J. Antibiot., Sec. A, 9*, 141.

Hingerty, B. E., Figueroa, S., Hayden, T., & Broyde, S. (1989) *Biopolymers 28*, 1195–1222.

Iyer, V. N., & Szybalski, W. (1963) *Proc. Natl. Acad. Sci. U.S.A. 50*, 355.

Live, D., Davis, D. G., Agosta, W. C., & Cowburn, D. (1984) *J. Am. Chem. Soc. 106*, 1939.

Norman, D., Abuaf, P., Hingerty, B. E., Live, D., Grunberger, D., Broyde, S., & Patel, D. J. (1989) *Biochemistry 28*, 7462–7476.

Olson, W. (1978) *Biopolymers 17*, 1015–1040.

Patel, D. J. (1974) *Biochemistry 13*, 2396–2402.

Patel, D. J. (1976) *Biopolymers 15*, 533–558.

Rao, S. N., Singh, U. C., & Kollman, P. A. (1986) *J. Am. Chem. Soc. 108*, 2058–2068.

Sklenar, V., & Bax, A. (1987) *J. Am. Chem. Soc. 109*, 7525.

Sklenar, V., Miyashiro, H., Zon, G., Miles, H. T., & Bax, A. (1986) *FEBS Lett. 208*, 94–98.

Srinivasan, A. F., & Olson, W. (1980) *Fed. Proc., Fed. Am. Soc. Exp. Biol. 39*, 2199.

States, D. J., Haberkorn, R. A., & Reuben, D. J. (1982) *J. Magn. Reson. 48*, 286–292.

Szybalski, W., & Iyer, V. N. (1967) in *Antibiotics I, Mechanism of Action* (Gottlieb, W., & Shaw, P. D., Eds.) pp 211–245, Springer, New York.

Teng, S. P., Woodson, S. A., & Crothers, D. M. (1989) *Biochemistry 28*, 3901–3907.

Tomasz, M., & Lipman, R. (1981) *Biochemistry 20*, 5056.

Tomasz, M., Lipman, R., Snyder, J. K., & Nakanishi, K. (1983) *J. Am. Chem. Soc. 105*, 2059–2063.

Tomasz, M., Lipman, R., Verdine, G. L., & Nakanishi, K. (1985) *J. Am. Chem. Soc. 107*, 6120–6121.

Tomasz, M., Lipman, R., Verdine, G. L., & Nakanishi, K. (1986a) *Biochemistry 25*, 4337–4344.

Tomasz, M., Chowdary, D., Lipman, S., Shimotakahara, S., Veiro, D., Walker, V., & Verdine, G. L. (1986b) *Proc. Natl. Acad. Sci. U.S.A. 83*, 6702.

Tomasz, M., Lipman, R., Chowary, D., Pawlak, J., Verdine, G. L., & Nakanishi, K. (1987a) *Science 235*, 1204–1208.

Tomasz, M., Lipman, R., Lee, M. S., Verdine, G. L., & Nakanishi, K. (1987b) *Biochemistry 26*, 2010–2027.

Tomasz, M., Lipman, R., McGuinness, B. F., & Nakanishi, K. (1988) *J. Am. Chem. Soc. 110*, 5982–5986.

Verdine, G. L. (1986) Ph.D. Thesis, Columbia University.

Wakaki, S., Marumo, H., Tomioka, K., Shimizu, G., Kata, E., Kamada, H., Kudo, S., & Fujimoto, Y. (1958) *Antibiot. Chemother. 8*, 288.

Webb, J. S., Cosulich, D. B., Mowat, J. H., Patrick, J. B., Broschard, R. W., Meyer, W. E., Williams, R. P., Wolf, C. F., Fulmor, W., Pidacks, C., & Lancaster, J. E. (1962) *J. Am. Chem. Soc. 84*, 3185–3186.

Weiner, S., Kollman, P., Nguyen, P., & Case, D. (1986) *J. Comput. Chem. 7*, 230–252.